Whole-brain functional and structural examination in larval zebrafish

Advisor: Prof. Florian Engert Author: David Grant Colburn Hildebrand

Whole-brain functional and structural examination in larval zebrafish

Abstract

Comprehending how neuronal networks compute is a central goal in neuroscience, but it is challenging to directly measure how information flows through and is processed by large circuits of interconnected neurons. Ideally, one would capture what every neuron represents and determine which of its counterparts this information was shared with. However, measuring neuronal activity requires high temporal resolution and finding the connections between neurons requires high spatial resolution. The constraints imposed by current techniques for evaluating neuronal population activity and network anatomy put these requirements at odds: those that sample rapidly typically do so with lower spatial resolution, while those that provide high spatial resolution generally sample slowly. Finding ways to combine the strengths of different approaches and applying them to relatively small nervous systems holds great potential for examining neuronal network function.

The translucence, genetic toolset, and small size of the larval zebrafish model organism make it ideal for whole-brain activity mapping at cellular resolution while presenting sensory stimuli and recording behavior. Constant improvements to reporters of neuronal activity and light microscope designs are being made to capture snapshots of neuronal activity more rapidly. However, existing methods for identifying neuronal connectivity in larval zebrafish are applicable to only a small fraction of the population at once. An efficient way to determine the neuronal network anatomy—or wiring diagram—of a circuit is to reconstruct connections from micrographs of continuous series of thin sections acquired with electron microscopy, but this

technique has yet to be applied to studying neuronal circuits in larval zebrafish. Furthermore, its use has not yet approached the scale of the complete larval zebrafish brain.

This dissertation describes new tools for enhancing larval zebrafish activity mapping endeavors and the development of a serial-section electron microscopy approach to accomplish dense structural imaging of the complete brain. Together, these developments provide a foundation for studying neuronal network computation in the context of a behaving animal.

For George Powers Dirth (1986–2013),
who understood all forms of fun.

Acknowledgments

Graduate school has been a fascinating experience. There are several people that played a part in this journey, and I would like to thank many of them here. Others will be mentioned in the text to indicate their specific contributions to this work.

My advisor, Florian Engert, invited me to join his group to work on a project for which I had little practical prior knowledge. His confidence in my ability to get the job done was motivating, especially when the experiments themselves were not. The provisions he supplied—food, espresso, and beer—and his good company always made the lab an enjoyable place. Most importantly, Florian showed by example that a successful principal investigator can foster a productive environment while treating his trainees and staff well, not taking himself too seriously, and having fun.

The other members of the Engert lab served as a great group of friends and colleagues throughout my time there. Despite the fact that I was almost always off in a different lab space, they treated me as they would any other lab member. I truly appreciate their willingness to teach me anything they knew and to consistently prioritize collaboration over competition.

None of this work would have been possible without the support of my collaborators in the Lichtman, Reid, and Schier labs. Prof. Jeff Lichtman, Prof. Clay Reid, and Prof. Alex Schier were insightful advisors, providing direction and helping to secure funding for my work. Ken Hayworth, Josh Morgan, Richard Schalek, and Bobby Kasthuri guided me through the process of preparing and sectioning samples for scanning electron microscopy. Wei-Chung Lee, Davi Bock, and Hyon Kim walked me through the process of preparing and sectioning samples for transmission electron microscopy. Peng Huang performed initial larval zebrafish tissue processing tests with me.

Several students, technicians, and volunteers also helped. George Plummer assisted with scanning electron microscopy acquisition. Connor Elkhill, Fernando Camacho Garcia, Andrew Cohen, George Plummer, Bobby Plummer, Alex Coda, Ala Haddad, Paige Lewis, Kristen Runci, Iris Odstrcil, Mariela Petkova, Pepa Petkova, Leon Lin, and Elena Glushenkova annotated data and performed neuron reconstructions. Many in this group were generously hosted by Wei-Chung Lee. I cannot thank Wei enough for being such a dedicated mentor without any official obligation or credit for his efforts.

Many key contributions to this work came from colleagues at other institutions. Art Wetzel at the Pittsburgh Supercomputing Center and Stephan Saalfeld at the Howard Hughes Medical Institute's Janelia Research Center made it possible to align electron micrographs. Won-Ki Jeong provided an escape to the Ulsan National Institute of Science and Technology in Korea for a summer, where I was able to learn more about image processing and form useful collaborations. Members from his group, in particular Quan Tran Minh and Woohyuk Choi, produced valuable automatic segmentation algorithms for and visualizations of datasets collected as a part of this dissertation.

Outside these direct collaborations, many others deserve to be recognized. JoAnn Buchanan sent me unpublished tissue processing protocols. Liz Benecchi spent weeks attempting high-pressure freezing experiments for preserving larval zebrafish tissue. Susumu Ito suggested the low-viscosity epoxy resin that mitigated many of my sectioning troubles. Hunter Elliot, Tiao Xie, and Brett Graham assisted me with image processing and computer programming. Daniel Berger produced software that was used to process wafer images. Ed Soucy and Joel Greenwood helped me design and build a variety of tools.

My dissertation advisory committee gave valuable input and direction. The core members, Elio Raviola, Rachel Wilson, and Josh Sanes, were always honest and often encouraging. The Program in Neuroscience provided a wonderfully supportive environment for my graduate studies, from heavily invested directors and course instructors to an adept administrator in Karen Harmin, who guided me through paperwork, scheduling, and more. The Harvard Center for Brain Science and its Neuroengineering Core, the Harvard Medical School Image and Data Analysis Core, the Harvard Medical School Orchestra High-Performance Compute Cluster, the National Institutes of Health, and the National Science Foundation provided resources for my graduate studies either directly or through supported facilities.

Finally, I would like to thank my family. My siblings have been there for me whether or not they understand my interests or my work. The selfless, unconditional encouragement my parents and their spouses have provided is responsible for anything and everything I have accomplished. Being born to this lot was like winning the lottery. I truly hope that I will find the strength to be as good to my own children in the future.

Table of Contents

List of Figures and Tables

Chapter 1

Introduction

1.1 Overview

The nervous system consists of a meshwork of interconnected neurons that are collectively responsible for a range of tasks. These include extracting information from the environment, managing the internal state of the animal, and eliciting the motor actions that constitute behaviors. Neurons accomplish these functions as networks by communicating with one another through finely tuned electrical and chemical signals conveyed by axons and dendrites, thin cable-like structures that project relatively long distances away from the cell nucleus.

Given that its responsibilities vary so broadly and require a dynamic system, it is not surprising that there are numerous specialized components of the nervous system. For example, many different types of neurons exist, including broad classes that excite or inhibit other neurons. These physiological properties combine with the number and strength of a neuron's connections with others to determine how signals propagate, resulting in processing of information as it passes through the network of neurons.

Comprehending neuronal network computation is a central goal in neuroscience, but assessing how information flows through and is processed by circuits of interconnected neurons is challenging. Ideally, one would capture the information each neuron represents and determine which others it was shared with. This would require recording each neuron's electrical and chemical activity, identifying its inherent properties, and finding each of the synapses it makes onto its counterparts. However, measuring neuronal signaling requires high temporal resolution and finding the connections between neurons requires high spatial resolution. This is particularly a problem in the brain—where neurons are densely concentrated and extend their axons and dendrites long distances—because the same methods that permit high temporal sampling yield

lower spatial resolution and vice versa. These current technical limitations force most studies to choose either to measure neuronal activity or to resolve connectivity in relatively small neuronal populations, therefore limiting their ability to identify relationships between neuronal network structure and function (Lichtman and Denk, 2011).

This dissertation describes new tools and approaches that can be employed to overcome many of these limitations through a combination of model organism choice and improved functional and structural imaging strategies.

The remaining portions of this chapter contain background information on why it is important to understand the links between the function of neuronal circuits and their underlying structure while considering challenges that stand in the way. It next explores insights gained from previous work before ending with a description of why the larval zebrafish is an excellent model organism choice for such studies.

Chapter 2 presents current strategies for optically measuring the physiological properties of neurons in larval zebrafish, where major improvements can be made, and the generation of new transgenic zebrafish toward accomplishing these goals.

Chapter 3 explores existing techniques for determining the structure of neuronal networks and their benefits and limitations, describes challenges unique to larval zebrafish, introduces a new approach that overcomes many of these difficulties, and presents a high-resolution atlas of a complete larval zebrafish brain accompanied its surrounding tissues.

Chapter 4 discusses the strengths and shortcomings of the methods described in this dissertation before considering the future outlook of their application with an emphasis on improvements yet to be made.

1.2 Dependence of neuronal network function on connectivity

Neurons receive input from others at specialized synaptic junctions. Upon receiving excitatory input that exceeds inhibitory input by enough to rise above an activation threshold, these signals are then transmitted electrically as action potentials throughout the post-synaptic neuron and on to downstream neurons (Kandel *et al.*, 2000). Though exceptions exist, this simplistic view of neuronal circuit operation applies for the majority of inter-neuronal signaling in that neurons that do not share synaptic contacts lack a conduit for communicating with one another directly. Knowledge of the interconnectivity between neurons in a network is therefore necessary to understanding how signals might propagate through it.

Additional complexity in the form of intrinsic neuronal properties (Llinás, 2014), variable synaptic strengths (Bliss and Lømo, 1973; Pozo and Goda, 2010), neuromodulatory chemical signaling (Marder *et al.*, 2014), ephaptic coupling (Anastassiou *et al.*, 2011), and neuron-glia interactions (Perea *et al.*, 2014) render connectivity alone insufficient for discerning exactly how a signal will cascade through a network. However, matrices of neuronal connectivity—which can be thought of as circuit wiring diagrams—provide useful constraints on the possibilities (Briggman and Bock, 2012; Bargmann and Marder, 2013).

The dependence of neuronal circuit function on connectivity has traditionally been studied by combining results across several physiological and anatomical experiments that sparsely sample the same brain region. For example, it has been shown that the mammalian neocortex has several stereotyped structural features including a laminar organization, characteristic excitatory and inhibitory neuron morphologies, and specific distributions of neuron types and synapses (Douglas and Martin, 2004). These results give an important overall impression of how excitation flows through cortical circuits, and additional physiological

characterization provides evidence that many of the identified morphological attributes are predictors of cortical circuit function (Shepherd *et al.*, 2005; Song *et al.*, 2005). However, each of these experiments can focus only on a narrow subset of neurons at a time, making it likely that some connections with important functional consequences are missed because they did not view the complete structure of the circuit and its physiology simultaneously. Furthermore, this view of the neocortex took decades to produce, in part because experiments that sample sparsely are low-throughput and in part because identifying trends across different studies is nontrivial.

While combining results across multiple experiments has been successfully applied to gain insight into how neuronal circuits operate, it is likely that a great deal can be learned from a more complete picture of the system. Overlaying recordings of neuronal activity with extensive connectivity diagrams for the same populations of neurons has the potential to further elucidate the mechanisms by which information is represented and transformed by neuronal circuits.

1.3 Examining the function and structure of neuronal circuits

The field of neuroscience is constantly improving as techniques revolutionize opportunities for examining the anatomy and physiology of neurons. Just as silver nitrate staining (Golgi, 1873) made the detailed morphological descriptions of neurons by Ramón y Cajal possible (Ramón y Cajal, 1904) and tungsten electrodes (Hubel, 1957) enabled Hubel and Wiesel to identify neurons that respond to specific features in visual space (Hubel and Wiesel, 1959), new methodologies continue to push the field forward.

Recently, substantial technological improvements have resulted in the ability to record neuronal activity from large populations of neurons (Deisseroth and Schnitzer, 2013). These advances include the development of multi-electrode arrays with many recording sites for

measuring the extracellular field potentials associated with action potentials (Spira and Hai, 2013) and the combination of improved fluorescent sensors of calcium flux (Grienberger and Konnerth, 2012; Looger and Griesbeck, 2012) and new fast microscopes (Keller and Ahrens, 2015). Together, these methods have made it possible to measure how activity dynamics in large neuron populations encode features of a sensory stimulus (Ohki *et al.*, 2005; Ohki *et al.*, 2006; Portugues *et al.*, 2014), correlate with motor movements (Orger *et al.*, 2008; Ahrens *et al.*, 2012; Shenoy *et al.*, 2013), and much more.

Of particular interest for simultaneously investigating structure and function are the optical imaging approaches. Electrode arrays provide high temporal resolution, but yield limited spatial information for the waveforms they capture and are typically more invasive than desired. As a consequence, electrodes can reveal a great deal about overall population dynamics, but piecing together how the architecture of the circuit influences its function is difficult with these tools. On the other hand, optical imaging of neuronal activity produces both temporal and spatial information (Davila *et al.*, 1973; Knöpfel *et al.*, 2006; Kerr and Denk, 2008). Researchers must strike a balance between imaging volume size and resolution depending on the capabilities of their microscope and the questions they wish to ask. However, it is possible to investigate the dynamics of structures as small as dendritic spines (Yuste *et al.*, 2000; Sabatini *et al.*, 2001) or as large as an entire brain of certain model organisms at the single-neuron scale (Ahrens *et al.*, 2013; Panier *et al.*, 2013; Portugues *et al.*, 2014; Prevedel *et al.*, 2014).

New and better microscope designs are pushing the speeds and volume sizes that can be acquired. These include laser-scanning multiphoton microscopes (Zipfel *et al.*, 2003) equipped with resonant scanners (Fan *et al.*, 1999), spatial light modulators (Nikolenko *et al.*, 2008), acousto-optic deflectors (Grewe *et al.*, 2010), spatiotemporal multiplexing (Cheng *et al.*, 2011),

and electrically tunable lenses (Grewe *et al.*, 2011) that speed up the scanning process or do so in pre-defined patterns (Katona *et al.*, 2012). Creative modifications to selective plane illumination microscopes (Huisken *et al.*, 2004; Keller *et al.*, 2008)—also referred to as light-sheet microscopes because a sheet of light is passed through the sample orthogonal to the imaging objective—recently enabled recording neuronal activity across entire brains of relatively small and transparent organisms at substantially faster rates than with laser-scanning techniques (Ahrens *et al.*, 2013; Panier *et al.*, 2013). The introduction of light-field microscopes (Levoy *et al.*, 2006) holds promise for imaging at rates constrained only by the available signal and the camera, though its spatial resolution is currently lower than afforded by other methods (Ahrens and Engert, 2015). This relatively new imaging technique has already been applied to imaging of activity in large neuron populations from small and transparent organisms (Prevedel *et al.*, 2014).

Similar to microscope enhancements, genetically encoded reporters are undergoing continuous engineering to make intracellular calcium dynamics clear on faster timescales and with larger fluorescence changes (Knöpfel, 2012; Tian *et al.*, 2012). Unlike synthetic indicators that diffuse away from an injection site, the genetically encoded nature of these sensors enables long-term recordings and delivery to specific populations of neurons (Looger and Griesbeck, 2012) ranging in size from the extents of a viral vector injection and infection (Davidson and Breakefield, 2003; Zhu *et al.*, 2009) to the whole-brain via the creation of stable transgenic lines (Higashijima *et al.*, 2003).

With all these excellent improvements in recording neuronal activity faster, at higher spatial resolution, and from more neurons, however, accessing large populations with light microscopy still yields spatiotemporal resolution that is insufficient for capturing the precise

flow of excitation throughout most complex neuronal circuits. What results is essentially a survey or map of activity at cellular resolution that is often linked to a particular stimulus or task. Though they provide an excellent view of how parts of the nervous system represent information, the ability of only these activity maps to describe the mechanisms by which neuronal circuits shape the flow of this information is generally restricted to the production of models that need then be tested in subsequent experiments.

An alternative way to extract more details about the circuit is to perform additional experiments in the same specimen during activity mapping. This is akin to a commonly used technique in which experimenters studying the electrophysiology of single a neuron identify its morphological characteristics by filling it with a dye during a recording session (Friedlander *et al.*, 1981), but instead applied through a variety of techniques to as many neurons as possible during or immediately after measuring population activity. For example, it is possible to examine connectivity by additionally imaging fluorescent labels delivered by viruses that only infect the neurons monosynaptically connected to a single targeted neuron (Wickersham *et al.*, 2007a; Wickersham *et al.*, 2007b; Beier *et al.*, 2011). With retrograde and anterograde options available, this enables identification of a neuron's inputs or its outputs. However, this method involves sampling sparsely and is therefore unlikely to produce an extensive connectivity diagram. It also can require days to weeks for the virus to spread before a later imaging session depending on how it is implemented, during which time changes may occur. Alternatively, experimenters can simultaneously use genetically encoded reporters and manipulators of neuronal activity. In this case, additional functional imaging is performed during the optically driven activation of a neuron or a small group of neurons (Packer *et al.*, 2013; Rickgauer *et al.*, 2014; Packer *et al.*, 2015). It remains to be seen how reliably population connectivity can be

extracted from analyses of correlation between optically driven activation and elicited calcium responses, but this method has great potential.

Another approach is to identify connections between neurons in *post hoc* experiments after careful correspondence of neuron identity with cellular-resolution activity maps. In this case, neuron somata can be registered between the datasets using landmarks such as blood vessels and the pattern of neuron placement throughout the tissue as guides (Knott *et al.*, 2009; Kerlin *et al.*, 2010). This procedure has been successfully applied to *in vitro* electrophysiology preparations to test for connections between neurons co-activated by presentation of the same visual stimulus (Ko *et al.*, 2011) and even to probe connection strength between them (Ko *et al.*, 2013). Producing an extensive connectivity matrix for a substantial proportion of the neurons whose activity was mapped is unlikely, however, because paired electrophysiological recordings are low-throughput and typically performed in slices of the sample containing neurons whose long-range connections are disrupted and whose viability diminishes with time.

The *post hoc* correspondence approach can also be used to combine activity mapping with electron microscopy (EM), a technique that affords high enough spatial resolution to visualize individual synaptic vesicles. Increasing the spatial resolution to this degree permits the staining and identification of many fine neuronal structures (Peters *et al.*, 1991), enabling the separation of thin adjacent axons or dendrites based solely on their cellular membranes rather than requiring sparse labeling strategies to resolve structures as required in light microscopy. Assembling a three-dimensional stack of images acquired from serial thin (~30–70 nanometers thick) sections of a sample makes it possible to follow the contours of axons and dendrites throughout a volume and determine where synapses between neurons occur. This technique has been applied to grasp the structure of neuronal circuit connectivity over scales ranging from

individual synapses (Hamos *et al.*, 1987; Sorra and Harris, 1998) to the entire nervous system of the nematode *Caenorhabditis elegans* (White *et al.*, 1986).

While serial-section EM has been combined successfully with electrophysiology for decades (Sterling, 1983; Dacheux and Raviola, 1986; Hamos *et al.*, 1987; Sorra and Harris, 1998), only recently has it been merged with functional imaging to produce connectivity diagrams alongside activity maps (Bock *et al.*, 2011; Briggman *et al.*, 2011). Application of this method to identify connections between functionally characterized neurons revealed important computational properties of neuronal circuits in both the mouse cortex and retina. In the cortex, it was confirmed that inhibitory interneurons received pooled input from excitatory pyramidal cell neurons that were active during the presentation of a broad range of differently oriented visual stimuli rather than only a specific set, suggesting that they may be setting the gain of the local excitatory microcircuit (Bock *et al.*, 2011). In the retina, it was discovered that an asymmetry that contributes to the computation of direction selectivity is formed by highly specific connectivity between starburst amacrine cells and direction-selective ganglion cells that depends on the latter's preferred direction (Briggman *et al.*, 2011).

These experiments were enabled by the ability to survey activity from large populations of neurons using light microscopy, the introduction of new electron microscope designs that resulted in high-throughput imaging or less error-prone sample handling, and the benefits of modern computer speed and data storage capabilities. While the combination of rapid, broad functional and dense structural imaging proved useful for extracting mechanistic details about the computations performed in each small circuit, additional improvements would permit scaling to even larger networks of neurons. This is important because many circuits span large brain volumes. For example, many neurons in the mouse cortex send projections across the brain to

the contralateral cortex while maintaining some specific rules of connectivity (Petreanu *et al.*, 2007). Mapping activity across neuron populations this large will require substantial improvements in calcium reporters, faster microscope technologies, or new approaches altogether (Marblestone *et al.*, 2013). Examining neuronal connectivity with serial-section EM at the whole-brain level in an organism of this size requires improved tissue preservation and staining (Mikula *et al.*, 2012), further automation of sample handling, and higher-throughput or parallel imaging setups (Eberle *et al.*, 2015).

However, applying only a handful of these improvements to a smaller model organism—such as a larval zebrafish (*Danio rerio*)—may make it possible to analyze structure-function relationships across a complete brain (Ahrens and Engert, 2015).

1.4 Studying neuronal network function and structure in larval zebrafish

Zebrafish were selected as a model system decades ago with the specific goal of studying development (Streisinger *et al.*, 1981). In addition to genetic advantages inherent to the organism, other features that led to this choice included its rapid development, the simultaneous production of many progeny by a single female, the small size and partial transparency of eggs and larvae, and the early emergence of behavior (Laale, 1977). This suite of characteristics resulted in the adoption of zebrafish for studying many organ systems and led to the establishment of several techniques for their use and care (Detrich III *et al.*, 1998; Nusslein-Volhard and Dahm, 2002). Further investigation of nervous system development and behavior soon led neurobiologists to join in studying zebrafish.

When synthetic calcium reporters became available, the partial transparency of larval zebrafish was readily exploited to accomplish *in vivo* imaging of small neuronal populations

(Fetcho and O'Malley, 1995; O'Malley *et al.*, 1996; Fetcho and O'Malley, 1997). With the introduction of genetically encoded activity reporters, the genetic tools developed for zebrafish were invaluable for the creation of stable transgenic lines with brain-wide expression of the sensors and resulted in more customary neuronal activity imaging (Higashijima *et al.*, 1997; Higashijima *et al.*, 2003). These experiments were further enhanced by the use of chemical compounds (Karlsson *et al.*, 2001) and the generation of mutant strains (White *et al.*, 2008) to reduce pigments that limit transparency as larval zebrafish age.

With the aforementioned improvements in microscope technology and optical activity reporters, it is now possible to capture a snapshot of activity in most of the approximately 100,000 neurons contained in the larval zebrafish brain once or twice per second (Ahrens *et al.*, 2013; Panier *et al.*, 2013; Portugues *et al.*, 2013; Feierstein *et al.*, 2014; Portugues *et al.*, 2014; Keller and Ahrens, 2015). These experiments can be performed in the context of a behaving animal by closed-loop presentation of visual stimuli updated with feedback from recorded tail movements in partially restrained larvae (Portugues *et al.*, 2014) or fictive movements deduced from electrophysiological motor nerve recordings in paralyzed larvae (Masino and Fetcho, 2005; Ahrens *et al.*, 2012; Vladimirov *et al.*, 2014). As a consequence of these efforts, mapping activity across the complete larval zebrafish brain while the animal behaves is already possible and will become even more informative with further improvements to reporters and microscopes.

Structural examination of the larval zebrafish nervous system with electron microscopy (EM) has primarily been used to examine structural features from restricted regions of the hindbrain (Kimmel *et al.*, 1981), posterior lateral line system (Metcalfe *et al.*, 1985; Pogoda *et al.*, 2006; Monk *et al.*, 2009), and retina (Schmitt and Dowling, 1994, 1999; Emran *et al.*, 2010). There are no known published examples of serial-section EM being applied to the larval

zebrafish nervous system but for ongoing efforts in small brain regions (Friedrich *et al.*, 2013). It is not clear if methods perfected for studying mammalian model organisms (Hayat, 1981) are sufficient for producing quality preservation of the neuronal ultrastructure across the entire larval zebrafish brain. However, the volumetric limits of currently available serial-section EM technologies are estimated at roughly the same size as the larval zebrafish brain (Helmstaedter *et al.*, 2008; Friedrich *et al.*, 2010; Briggman and Bock, 2012), implying that it is—at least in theory—possible to capture complete neuronal circuits using current serial-section EM technologies.

This dissertation details a methodological approach for taking advantage of the larval zebrafish model organism to study the relationship between neuronal circuit structure and function. Chapter 2 describes the improvements to activity mapping capabilities through the generation of stable transgenic zebrafish expressing more sensitive, faster fluorescent reporters of calcium activity. Chapter 3 details a new framework for producing serial-section EM datasets spanning the complete larval zebrafish brain. Chapter 4 then investigates ways in which these methods improved to better address the questions for which they were designed.

Chapter 2

Generation of transgenic zebrafish expressing improved calcium indicators

2.1 Introduction

The most commonly used optical indicators of neuronal population activity are calcium indicators, which track changes in intracellular calcium levels with variations in fluorescence. These serve as an indirect measurement of electrical activity by relying on the voltage-gated calcium channels present in most neurons, which open upon sufficient membrane potential depolarization—such as during an action potential—and result in an increase intracellular calcium concentration (Jaffe *et al.*, 1992; Grewe and Helmchen, 2009; Grienberger and Konnerth, 2012). Calcium dynamics are slower than their underlying voltage changes, resulting in signal integration that yields high dynamic range but fundamentally restricts the temporal resolution with which neuronal activity can be measured. Voltage indicators that track changes in membrane potential with variations in light intensity are being developed to provide a direct measurement of a neuron's electrical activity similar to electrophysiological recordings. These would be preferable as a direct and faster readout of neuronal activity, but they are not yet mature enough for cellular resolution population recordings (Looger and Griesbeck, 2012).

Synthetic small molecule calcium indicators have undergone optimization for decades. The products of this work—namely Oregon Green BAPTA-1 (OGB) and fluo-4—have high signal-to-noise ratios and can rapidly track calcium concentration fluctuations as a result of being photostable, having high affinity for calcium, and displaying large fluorescence changes upon interaction with calcium. As a result, these indicators have provided a wealth of information about neuronal population dynamics (Knöpfel *et al.*, 2006; Grienberger and Konnerth, 2012; Looger and Griesbeck, 2012). However, synthetic dyes are generally injected as a large bolus into the extracellular space, an invasive procedure that results in high background signal, uneven distribution of the indicator in the tissue, and diffusion away from the recording site over time

that prevents long-term recordings. Genetically encoded, protein-based calcium indicators were introduced to counteract these problems, to enable targeting to specific classes of neurons, and to facilitate the creation of transgenic animals with pan-neuronal indicator expression (Looger and Griesbeck, 2012).

Until recently, genetically encoded calcium indicators were not able to match the sensitivity and speed of their synthetic counterparts, thereby forcing experimenters to compromise and choose which parameters were most important to them. Nonetheless, changes in both single-fluorophore and fluorescence resonance energy transfer-based families of genetically encoded sensors have steadily increased their capabilities over time. In particular, the GCaMP family of single-fluorophore reporters (Nakai *et al.*, 2001)—consisting of fused green fluorescent protein, calmodulin, and a peptide from the myosin light chain kinase—has gone through several iterations of rational and structure-guided modifications (Tian *et al.*, 2009; Muto *et al.*, 2011; Akerboom *et al.*, 2012) resulting in it becoming the most commonly used.

Application of a brute-force, high-throughput mutagenesis approach with screening in neurons recently provided a breakthrough set of three "GCaMP6" indicators with performance similar to the best synthetic indicators (Chen *et al.*, 2013). Of these variants, the one with the fastest kinetics (rise and decay times), called GCaMP6f, is comparable to OGB both in its sensitivity and speed, thus dramatically improving the ability to decode individual action potentials from calcium traces. A slower variant, called GCaMP6s, is substantially more sensitive, with action potentials resulting in seven-fold greater normalized fluorescence signals than obtainable with GCaMP5G, the best genetically encoded indicator prior to GCaMP6 and the last for which a stable transgenic zebrafish line was made. All of the advances provided by the

GCaMP6 indicators have the potential to substantially improve whole-brain activity mapping experiments in larval zebrafish.

This chapter describes the process by which a stable transgenic zebrafish line with nearly pan-neuronal GCaMP6f was created, beginning with molecular cloning and ending with proof-of-concept calcium imaging experiments. It also briefly reports additional reagents produced to facilitate examination of the relationship between structure and function in neuronal circuits.

2.2 Producing transgenic zebrafish with nearly pan-neuronal GCaMP6f expression

2.2.1 Molecular cloning

The process of generating a stable transgenic zebrafish line expressing GCaMP6f (Chen *et al.*, 2013) in almost every neuron started with molecular cloning of the GCaMP6f gene. The goal of this cloning step was to incorporate GCaMP6f into a *Tol2* site-containing plasmid, part of a transposon system that is commonly used for high-efficiency integration into the zebrafish genome (Kawakami, 2007).

The pGP-CMV-GCaMP6f plasmid containing the GCaMP6f gene was ordered from a repository (Addgene 407553), where it had been generously donated by its creators prior to its publication. Primers for PCR amplification of the GCaMP6f open reading frame were designed to be compatible with "cut and paste" cloning (restriction digest followed by ligation) into a Gateway® destination vector (pDest; Invitrogen, now Life Technologies) previously modified to contain *Tol2* sites (Ahrens *et al.*, 2012). Restriction sites in the target region of pDest, directly downstream of a Gateway® attR site, included SpeI and SacII. Sequences consisting of these restriction sites were added to the PCR primers flanking the template-matching nucleotide region, resulting in forward primer

5' – ataACTAGTgccaccATGGGTTCTCATCATCAT – 3'

and reverse primer

5' – ataCCGCGGcTCACTTCGCTGTCATCATTTGTAC – 3'

with restriction sites and coding sequences listed in upper case, respectively. PCR amplification of the GCaMP6f open reading frame (Figure 2.1a) was followed by a restriction digest with the SpeI and SacII restriction endonucleases (New England BioLabs). The destination vector pDest was subjected to the same restriction digest. DNA ligation was then performed to insert the PCR-amplified GCaMP6f fragment into the destination vector (TaKaRa DNA Ligation Kit, Clontech Laboratories), yielding the pDest-GCaMP6f vector (Figure 2.1b). As with all cloning steps, the produced plasmid was selectively cultured in bacteria by presentation of the appropriate antibiotic(s) for which it contained genes conveying resistance. The resulting pDest-GCaMP6f plasmid was subjected to sequencing in order to ensure this cloning step was successful without errors before proceeding onto the next step.

The new destination vector pDest-GCaMP6f contains *Tol2* sites that enable efficient genome integration and the GCaMP6f open reading frame, but lacks a promoter for driving expression. The previously described *elavl3* (*HuC*) *cis*-regulatory elements (Kim *et al.*, 1996) comprise the most common promoter used to accomplish practically pan-neuronal expression in zebrafish (Higashijima *et al.*, 2003; Ahrens *et al.*, 2012; Ahrens *et al.*, 2013). A modified Gateway® entry vector (pEntry; Invitrogen, now Life Technologies) containing the *elavl3* (*HuC*) promoter flanked by Gateway® attL sites had been created previously (Ahrens *et al.*, 2012). This permitted placement of the promoter directly upstream of GCaMP6f via LR recombination (Invitrogen, now Life Technologies), which essentially swaps the DNA elements between the attL sites in pEntry-HuC with the DNA between the attR sites in pDest-GCaMP6f through

recombination (Figure 2.1c). The resulting *Tol2*-*elavl3*-GCaMP6f-*Tol2* plasmid was then ready for the next step in creating a transgenic zebrafish line, injection into fertilized embryos.

Analogous cloning was also performed to produce a variety of additional *Tol2* site-containing plasmids for later creation of stable transgenic zebrafish lines that are likely to be useful for investigating the relationship between neuronal circuit structure and function. Table 2.1 summarizes the resulting plasmids and their potential uses.

Figure 2.1 — Strategy for generating stable transgenic zebrafish lines.

a, PCR amplification of the gene of interest, in this case GCaMP6f (Chen *et al.*, 2013), with primers that contain restriction sites compatible with the target plasmid.

b, Cut-and-paste cloning of the PCR-amplified GCaMP6f fragment into a *Tol2* destination vector (pDest).

c, Gateway® cloning reaction to achieve insertion of the promoter sequence, in this case for the *elavl3 cis*-regulatory elements, into the pDest-GCaMP6f plasmid.

d, Co-injection of the expression vector, *Tol2*-*elavl3*-GCaMP6f-*Tol2* and *Tol2* transposase mRNA into single-cell–stage embryos results in integration into the genome. Embryos are then nurtured to mating maturity and screened for germline integration, as indicated by F1 progeny with GCaMP6f expression.

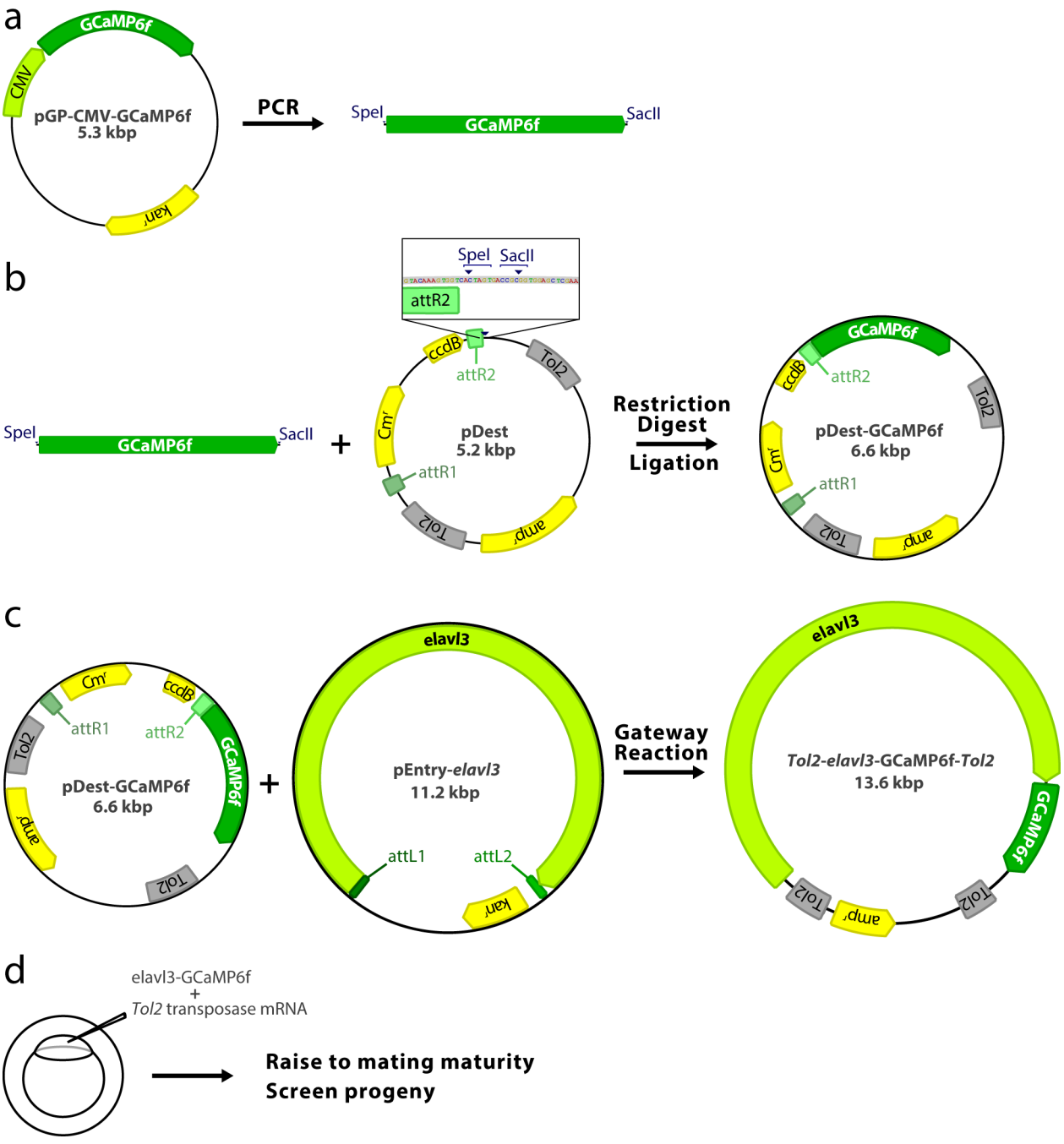

Figure 2.1 (continued)

Table 2.1 — A list of generated plasmids, the purpose for which they were created, and a reference pertaining to the source of the integrated construct.

Generated Plasmid	Purpose	Reference
pDest-GCaMP6f	Rapid, high-sensitivity calcium imaging	Chen *et al.*, 2013
Tol2-elavl3-GCaMP6f-*Tol2*		
pDest-GCaMP6m		
Tol2-elavl3-GCaMP6m-*Tol2*		
pDest-GCaMP6s		
Tol2-elavl3-GCaMP6s-*Tol2**		
pDest-PATagRFP-N1	Photoconvertable off-to-red fluorophore for light-based neuron labeling at specific time points during development	Subach *et al.*, 2010
pDest-PATagRFP-tubulin		
Tol2-elavl3-PATagRFP-N1-*Tol2*†		
Tol2-UAS-PATagRFP-N1-*Tol2*		
Tol2-elavl3-PATagRFP-tubulin-*Tol2*		
pDest-miniSOG	Genetically encoded label for electron microscopy	Shu *et al.*, 2011
pDest-tdminiSOG		
pDest-iLOV	Fluorophore that survives tissue processing for electron microscopy for correlated light and electron microscopy	Chapman *et al.*, 2008
pDest-magA	Possible genetically encoded label for electron microscopy‡	Nakamura *et al.*, 1995
pEntry-Hcrt	Promoter for isolated population of neurons for simplified testing of electron microscopy labels	Prober *et al.*, 2006

*Generation of a stable transgenic line with this plasmid was conducted by Abhinav Grama.

†This plasmid was used to generate a stable transgenic line, data not shown.

‡The idea for using magA as a label in electron microscopy came from Loren L. Looger.

2.2.2 Injection and screening

The next requirement for creating a stable transgenic zebrafish line is to accomplish germline integration of the cloned DNA construct into the zebrafish genome. For this, the *Tol2* transposon system is crucial, as it increases the efficiency of injected embryos producing transgenic offspring to ~50% from ~5% with DNA injection alone (Kawakami, 2007). To this end, 30 ng×μL^{-1} of the *Tol2*-*elavl3*-GCaMP6f-*Tol2* plasmid was co-injected with 30 ng×μL^{-1} *Tol2* transposase mRNA into several fertilized, single-cell stage embryos (Figure 2.1d). The injected embryos were then grown to mating maturity (2.5-3 months post-fertilization).

Upon reaching adulthood, these zebrafish were out-crossed to nacre (*mitfa*$^{-/-}$) fish, which are more transparent because their skin lacks certain pigments (White *et al.*, 2008). The resulting embryos were screened at ~2 days post-fertilization, a point in development when *elavl3*-driven expression is particularly strong. Progeny from this F1 generation that displayed bright GCaMP6f expression throughout the brain when examined with a wide-field fluorescence microscope were isolated and nurtured to mating maturity. Upon screening the progeny of this generation, a single F1 founder was selected based on high and spatially broad expression in its offspring. Outcrossing this founder generated ~50% *elavl3*-GCaMP6f–positive embryos, which were raised to establish the *Tg(elavl3:GCaMP6f)a12200* line. All of this injection and screening work was carried out in collaboration with Isaac H. Bianco.

2.2.3 Characterization

Observing bright, brain-wide green fluorescence for the *Tg(elavl3:GCaMP6f)a12200* line through a wide-field fluorescence microscope was a good indication that the *elavl3*-GCaMP6f construct was inserted into a region of the genome that facilitated expression in neurons.

However, nearly pan-neuronal expression is a prerequisite for whole-brain activity mapping and there may be positional effects that lead to undesirable variegated expression patterns if the artificially introduced promoter is adversely influenced by the regulatory environment surrounding sites where integration occurs (Roberts *et al.*, 2014). It is therefore important to gauge expression patterns with a method that affords higher spatial resolution.

To ensure that the *Tg(elavl3:GCaMP6f)a12200* line accomplished near-complete, pan-neuronal expression of GCaMP6f, it was qualitatively compared to a stable transgenic known to exhibit expression in almost every neuron. The *Tg(elavl3:H2B-mRFP)a9486* line (generated by Clemens Riegler) was chosen, as it expresses a red fluorescent protein in the nucleus of nearly all neurons. GCaMP6f is excluded from the nucleus but diffuses out into axons and dendrites, thus densely labeling neuropil regions. Because H2B-mRFP is restricted to the nucleus, it provides a clearer view of where individual neurons are located. One can then identify if signal in the green GCaMP6f channel is present around each identified nucleus.

In order to visualize GCaMP6f and H2B-mRFP in the same specimen, the two lines were crossed together to yield double-transgenic offspring heterozygous for each transgene. Upon reaching 5 days post-fertilization, the larvae were paralyzed with α-bungarotoxin and embedded in low-melting-point agarose inside a glass capillary tube. This preparation enabled simultaneous dual-channel imaging of the complete brain in a Zeiss Lightsheet Z1 microscope. Image stacks resulting from 3 larval zebrafish were used to qualitatively compare expression. As an initial test, z-projections were used to flatten the whole-brain image volumes into a single image. As expected, regions of the brain known to have high somata densities appeared as darker bands than dense neuropil regions in the GCaMP6f channel and as tightly packed puncta in the H2B-mRFP channel (Figure 2.2). A closer, plane-by-plane survey further confirmed that nearly

Figure 2.2 — Initial characterization of GCaMP6f expression throughout the brain in a double-transgenic 5 days post-fertilization Tg(*elavl3*:GCaMP6f; *elavl3*:H2B-mRFP) larval zebrafish with light-sheet microscopy.

a, Bright-field image for orientation.

a′, Standard deviation *z*-projection of GCaMP6f signal throughout the brain.

a″, Standard deviation *z*-projection of H2B-mRFP signal throughout the brain. Consistent with nearly pan-neuronal expression, regions of the brain known to have high somata densities appear as darker bands than dense neuropil regions in the GCaMP6f channel and as tightly packed puncta in the H2B-mRFP channel.

Scale bars, 250 μm.

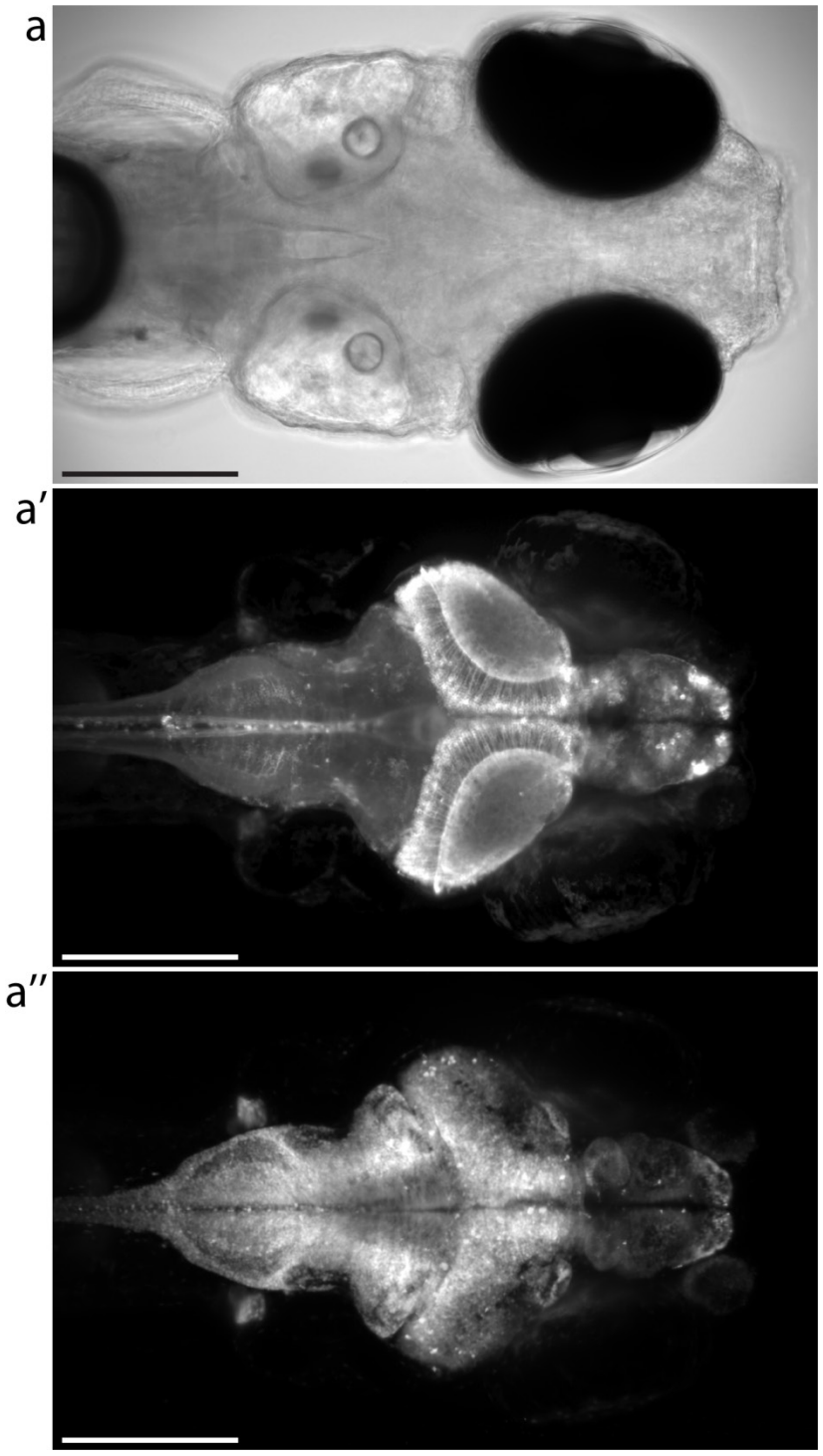

Figure 2.2 (continued)

pan-neuronal expression had been achieved with the *Tg(elavl3:GCaMP6f)a12200* line, as neuronal nuclei indicated by H2B-mRFP were surrounded by cytosolic GCaMP6f in all observed cases (Figure 2.3).

The goal of producing a zebrafish line with whole-brain GCaMP6f expression was to measure neuronal activity. It is therefore important to perform calcium imaging tests with the *Tg(elavl3:GCaMP6f)a12200* line to ensure that the GCaMP6f construct inserted into the genome is functional. To this end, brief whole-brain activity mapping experiments were conducted in collaboration with Misha B. Ahrens using a custom-built light-sheet microscope, which permits simultaneous calcium imaging and presentation of a visual stimulus (Vladimirov *et al.*, 2014). Whole-brain image stacks with 0.406 μm × 0.406 μm × 8.0 μm voxels were produced at a rate of 1.93 Hz while paralyzed larval zebrafish were shown whole-field gratings. The gratings switched between moving or stationary states with a period of ~10 sec (20 frames). Moving gratings are a stimulus known to elicit the optomotor response in larval zebrafish, in which a freely moving animal will turn to orient itself in the direction of the moving gratings and swim along with the movement (Portugues and Engert, 2009). During these imaging trials, variable GCaMP6f fluorescence consistent with fluctuations in neuronal activity was witnessed in many neurons (Figure 2.4). While the stimulus presentation was open-loop and not time-locked to the imaging, responses with a period of ~10 sec that were consistent with intended optomotor response-induced swimming events were visible in the hindbrain (Figure 2.4b), an area known to contain movement initiate centers. More irregular, transient responses were present in forebrain areas that are known to exhibit high levels of spontaneous activity (Figure 2.4c). These initial imaging experiments confirm that the *Tg(elavl3:GCaMP6f)a12200* line expresses a functional GCaMP6f calcium reporter.

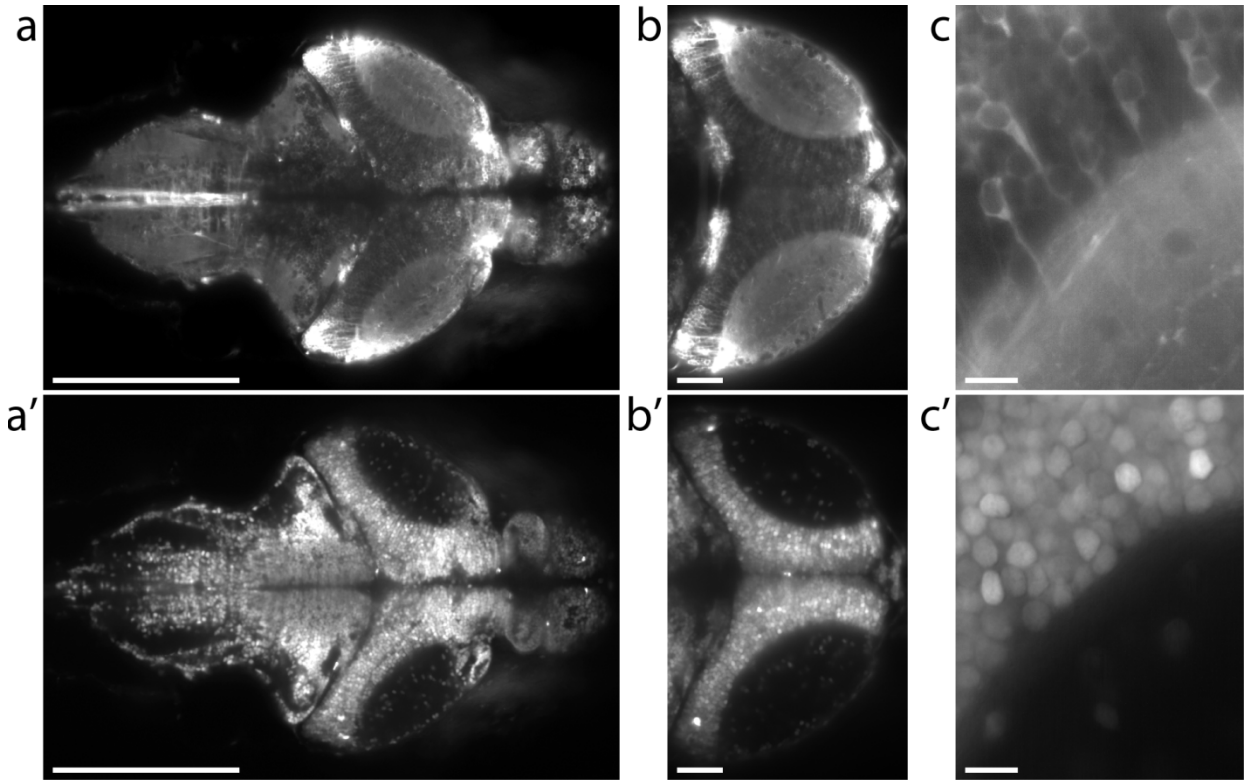

Figure 2.3 — Examples from surveying GCaMP6f expression in a 5 days post-fertilization Tg(*elavl3*:GCaMP6f; *elavl3*:H2B-mRFP) larval zebrafish with light-sheet microscopy.

a-a′, GCaMP6f and H2B-mRFP signal from a single plane is consistent with nearly pan-neuronal expression. Regions rich in neuron somata appear as dim bands in the GCaMP6f channel, while neuropil regions are brighter. The opposite pattern is observed for the H2B-mRFP channel.

b-b′, Similar GCaMP6f and H2B-mRFP expression is observed in a more superficial plane of the optic tectum.

c-c′, Cytosolic GCaMP6f signal is visible surrounding each observed neuronal nucleus identified by H2B-mRFP expression.

Scale bars, 250 μm (**a-a′**), 50 μm (**b-b′**), 10 μm (**c-c′**).

Figure 2.4 — Calcium imaging experiments confirm integration of a functional GCaMP6f construct. Imaging performed in a paralyzed 5 days post-fertilization *Tg(elavl3:GCaMP6f)a12200* larval zebrafish with light-sheet microscopy. Each snapshot of GCaMP6f signal throughout the complete brain was acquired in ~0.52 sec (1.93 Hz acquisition). Whole-field gratings were presented during imaging and switched between moving or stationary states with a period of ~10 sec (20 frames).

a, Maximum intensity projection through 29 planes averaged over the duration of the imaging experiment for localizing neurons. Colored outlines correspond to regions shown in **b** and **c**.

b, GCaMP6f signal in the hindbrain varies over time in a manner consistent with expected neuronal activity in this region.

c, GCaMP6f signal in the forebrain varies over time and is consistent with spontaneous activity. Scale bars, 250 μm (**a**), 25 μm (**b-c**).

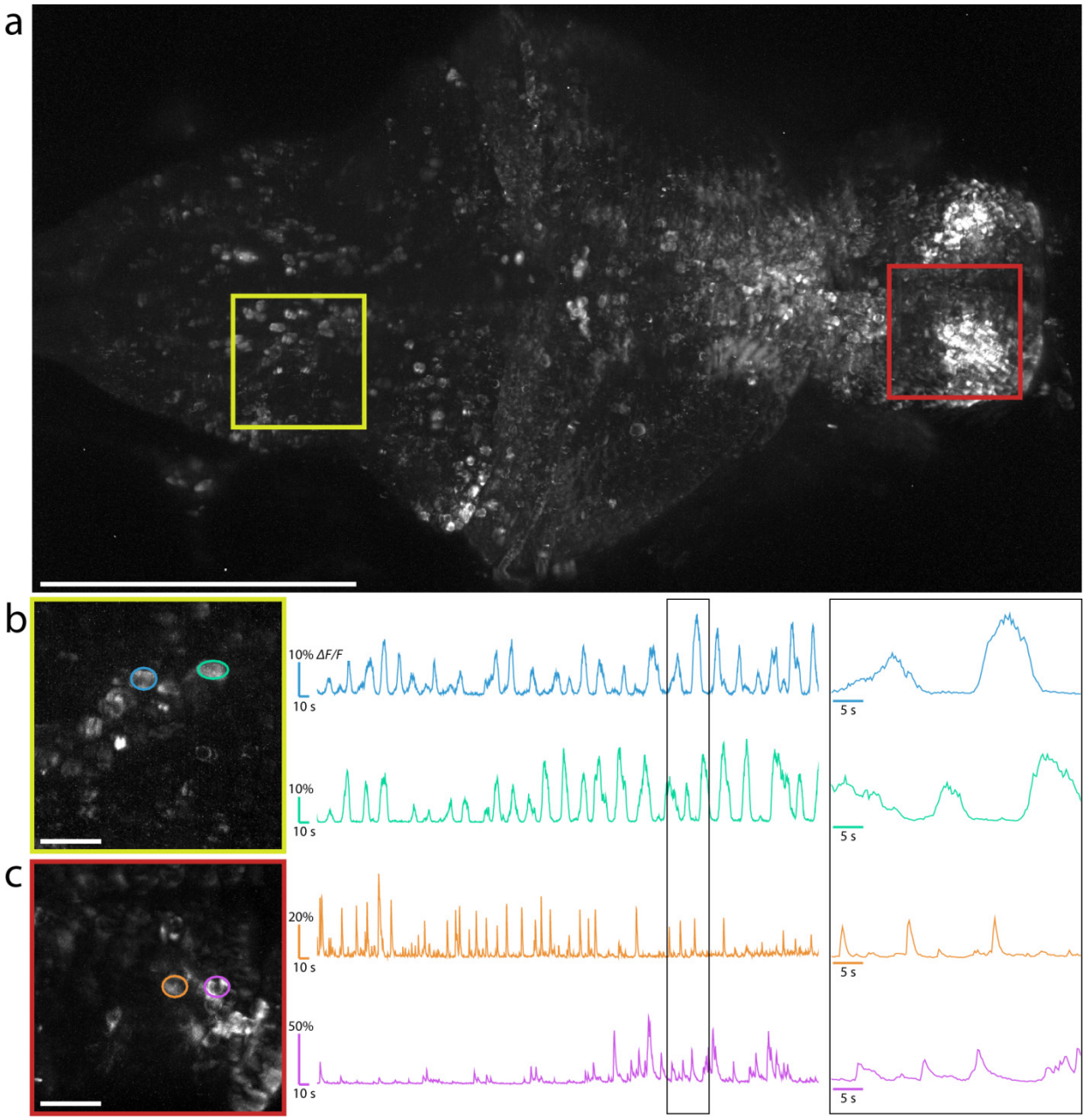

Figure 2.4 (continued)

2.3 Conclusions

This chapter described the production of genetic constructs and the generation of the *Tg(elavl3:GCaMP6f)a12200* stable transgenic zebrafish line to improve activity mapping experiments. This line is a new tool that enhances studies of structure-function relationships in neuronal circuits.

In addition to the described *Tg(elavl3:GCaMP6f)a12200* stable transgenic zebrafish line produced from the *Tol2-elavl3*-GCaMP6f-*Tol2* plasmid, a similar process was followed to generate and validate the *Tg(elavl3:PATagRFP-N1)a10573* line from the *Tol2-elavl3*-PATagRFP-N1-*Tol2* plasmid. This line provides an alternative for currently available transgenic lines that permit *in vivo* labeling of neurons but require the green channel, therefore making it difficult to simultaneously conduct calcium imaging experiments. With this option now available, it should be possible to conduct concurrent dual-channel calcium imaging and specific labeling of small populations of neurons via red fluorophore photoactivation for *in vivo* reconstruction of neuron morphologies or developmental studies.

Furthermore, many of the genetic constructs listed in Table 2.1 have been shared with collaborators, resulting in the generation of additional stable transgenic zebrafish. For example, Abhinav Grama used the *Tol2-elavl3*-GCaMP6s-*Tol2* plasmid to generate the *Tg(elavl3:GCaMP6s)a13203* line, which enables yet higher sensitivity calcium imaging at slower rates. Expression patterns for this line are similar to the *Tg(elavl3:GCaMP6f)a12200* line (Figure 2.5 and 2.6), serving as cross-confirmation for practically pan-neuronal expression in both transgenic zebrafish lines.

Finally, the *Tg(elavl3:GCaMP6f)a12200* line has been shared with several laboratories and is now frequently used for calcium imaging experiments. It was recently submitted for publication in collaboration with one of these groups (Cheng *et al.*, under review).

Figure 2.5 — Initial characterization of expression of GCaMP6s throughout the brain in a double-transgenic 5 days post-fertilization Tg(*elavl3*:GCaMP6s; *elavl3*:H2B-mRFP) larval zebrafish with light-sheet microscopy. The *Tg(elavl3:GCaMP6s)a13203* line was generated by Abhinav Grama from the *Tol2*-*elavl3*-GCaMP6s-*Tol2* plasmid (see Table 2.1).

a, Bright-field image for orientation.

a′, Standard deviation *z*-projection of GCaMP6s signal throughout the brain.

a″, Standard deviation *z*-projection of H2B-mRFP signal throughout the brain. Consistent with nearly pan-neuronal expression, regions of the brain known to have high somata densities appear as darker bands than dense neuropil regions in the GCaMP6s channel and as tightly packed puncta in the H2B-mRFP channel.

Scale bars, 250 μm.

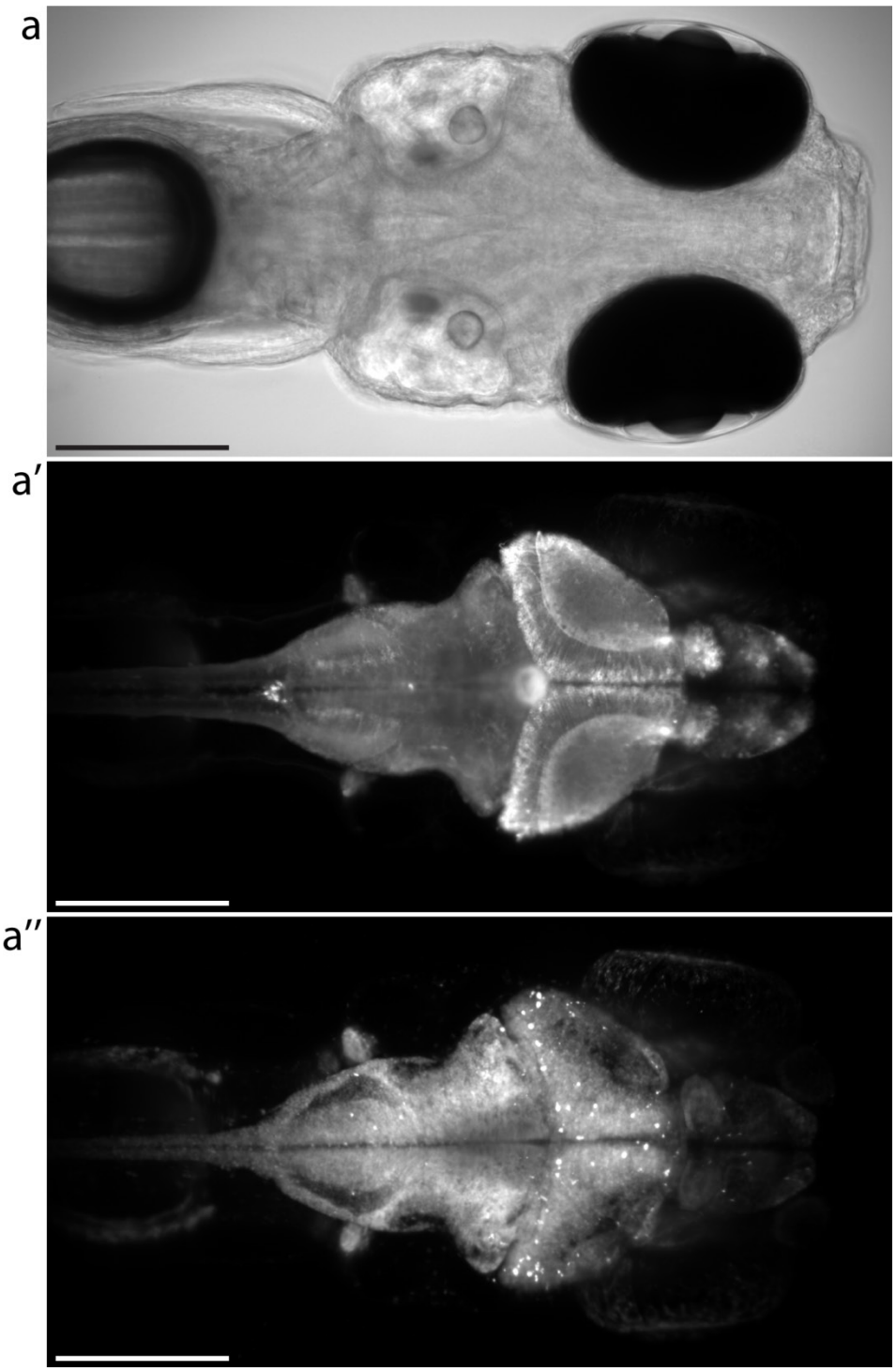

Figure 2.5 (continued)

Figure 2.6 — Surveying GCaMP6s expression in a 5 days post-fertilization Tg(*elavl3*:GCaMP6s; *elavl3*:H2B-mRFP) larval zebrafish with light-sheet microscopy. The *Tg(elavl3:GCaMP6s)a13203* line was generated by Abhinav Grama from the *Tol2-elavl3*-GCaMP6s-*Tol2* plasmid (Table 2.1). GCaMP6 expression in the *Tg(elavl3:GCaMP6f)a12200* and *Tg(elavl3:GCaMP6s)a13203* lines appears consistent, providing support for nearly pan-neuronal expression in each line despite the likelihood of different genome integration sites.

a-**a′**, GCaMP6s and H2B-mRFP signal from a single plane is consistent with practically pan-neuronal expression. Regions rich in neuron somata appear as dim bands in the GCaMP6s channel, while neuropil regions are brighter. The opposite pattern is observed for the H2B-mRFP channel.

b-**b′**, Similar expression of GCaMP6s and H2B-mRFP in a more superficial plane of the optic tectum.

c-**c′**, Cytosolic GCaMP6s signal is visible surrounding each observed neuronal nucleus identified by H2B-mRFP expression.

Scale bars, 250 μm (**a**-**a′**), 50 μm (**b**-**b′**), 10 μm (**c**-**c′**).

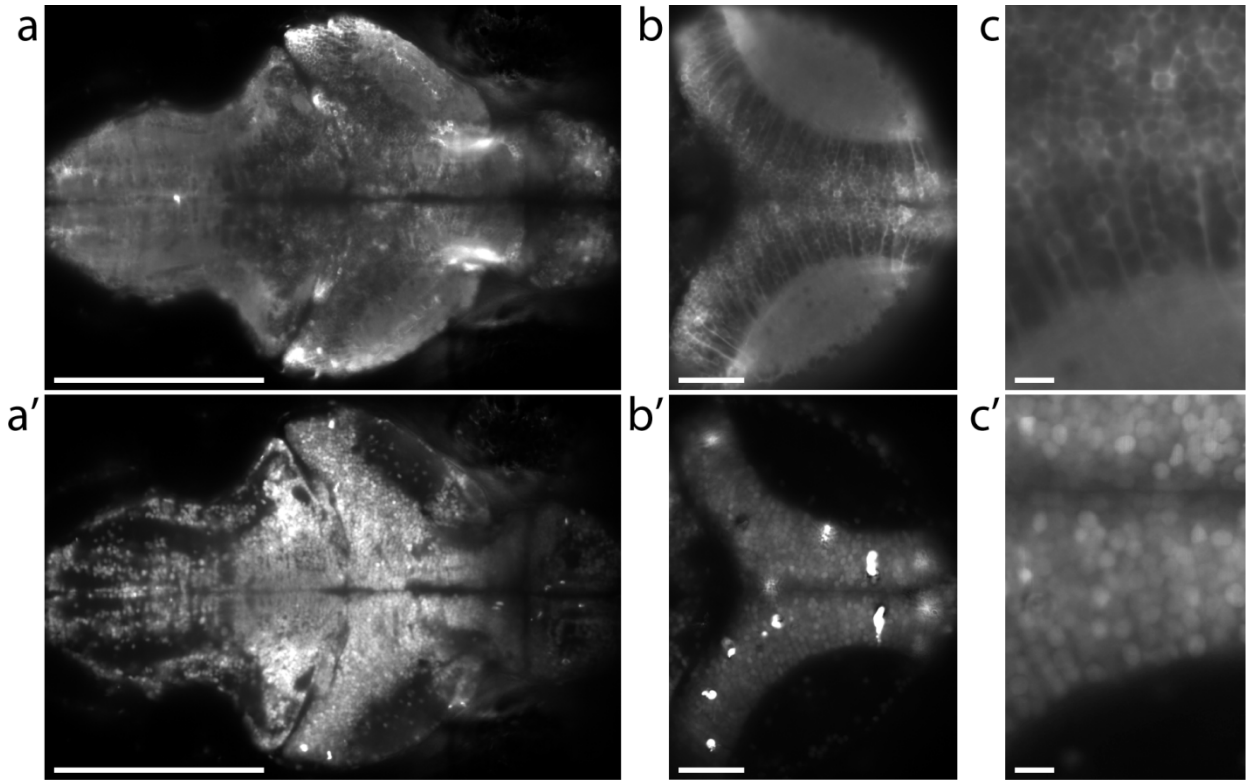

Figure 2.6 (continued)

Chapter 3

Whole-brain serial-section electron microscopy in larval zebrafish

3.1 Introduction

Generating datasets for detailed connectivity analysis is an important step toward understanding the relationships between neuronal circuit function and structure. The high spatial resolution afforded by electron microscopy (EM) makes it possible to investigate the densely packed neuronal processes and synapses that form neuronal circuits (Lichtman and Denk, 2011; Briggman and Bock, 2012). However, the imaging scale required to reliably reconstruct the paths of many axons and dendrites is ≥10 orders of magnitude smaller than the spatial extents occupied by complex networks of interconnected neurons—some of which span nearly the entire brain. The generation and management of data obtained by nanoscale imaging of relatively large volumes has thus confined most studies to neuron pairs or axon and dendrite fragments until recently. These efforts have now been transformed by computing advances and the development of larger-scale serial-section EM techniques (Denk and Horstmann, 2004; Anderson *et al.*, 2011; Bock *et al.*, 2011; Briggman *et al.*, 2011; Helmstaedter *et al.*, 2013; Hayworth *et al.*, 2014), but examining complete network connectivity across entire brains has remained a challenge.

Traditional serial-section EM required manual collection of thin sample partitions onto fragile film-covered slot grids followed by imaging with a transmission EM (Sterling, 1983; Dacheux and Raviola, 1986; White *et al.*, 1986; Hamos *et al.*, 1987; Sorra and Harris, 1998). At the time most of these studies were carried out, manual handling of photographs and other physical data forms was a difficult task. The assistance of increasing computer storage capabilities and the ease of visualizing digitally stored data have resulted in renewed interest in serial-section EM datasets of substantially larger tissue volumes.

New methodologies have made acquisition of such datasets possible, primarily through automation of sample handling and faster imaging. One major problem experienced with

traditional serial-section EM was labor-intensive manual serial sectioning and data loss due to tearing of film-covered slot grids. Unlike transmission EM, where a wide beam of electrons is passed through the thin section and therefore requires placement on a thin electron-lucent substrate, scanning electron microscopes raster a focused electron beam across a sample and detect electrons primarily from its surface. This makes it possible to perform block-face imaging of only the surface of an intact sample. A thin layer can then be removed from the top of the specimen before the next image is acquired by inserting a microtome into the microscope (Denk and Horstmann, 2004). Similarly, a focused ion beam can be used to remove a very thin layer from the block surface (Knott *et al.*, 2008).

These block-face imaging approaches greatly improve sample handling efficiency and reduce accidental losses. However, because the surface of the block is removed after each round of imaging, it is not possible to return to the sample for re-imaging or extraction of additional information using methods such as immuno-EM. As a consequence, the entire sample must be imaged at high spatial resolution from the start, preventing lower-resolution surveying and later high-resolution targeting. This is particularly an issue for large volumes such as a complete larval zebrafish brain, where one may wish to check ultrastructure preservation quality throughout the sample before committing many months or even years to its complete imaging.

Scanning EM can also be combined with physical serial sectioning onto substrates that are stable under an electron beam such as Kapton® polyimide tape (Dupont) using automated tape-collecting ultramicrotomes (Hayworth *et al.*, 2006; Schalek *et al.*, 2011; Hayworth *et al.*, 2014; Kasthuri *et al.*, under review). Collected sections persist on the tape substrate and can be imaged multiple times. While many scanning EM technologies are not as fast as inherently parallel transmission-based counterparts that are being modified for yet higher throughput (Bock

et al., 2011), new methods are being developed to improve scanning EM throughput through, for example, increased staining density (Tapia *et al.*, 2012) and parallel rastering of multiple beams (Eberle *et al.*, 2015).

Together, the advantages of simplified sample handling, multiple rounds of imaging, and rapidly improving imaging technologies position the combination of automated tape-collected microtomes and scanning EM at the forefront of large-scale EM endeavors. If applied to the whole larval zebrafish brain, these methods should make it possible to join whole-brain structural examination with whole-brain activity mapping.

3.2 Preparation of larval zebrafish for electron microscopy

3.2.1 Ultrastructure preservation and tissue processing

Serial-section EM of relatively large tissue volumes requires optimization of fixation, staining, embedding, and sectioning protocols. While tissue preparation protocols for EM of mammalian tissues are well-established (Hayat, 1981), applying these existing methods to the larval zebrafish model is not always straightforward. For example, aldehyde fixatives are typically delivered rapidly to the mammalian brain before anoxic conditions arise by means of *trans*-cardial vascular perfusion. Immersion of an entire mammal into a bath of fixatives would result in well-preserved skin, but the dura mater and skull would prevent fixative solutions from contacting the brain quickly enough.

Although larval zebrafish are substantially smaller than mammals, similar membranes that cover the brain (Miner and Yurchenco, 2004; Xiao and Baier, 2007; Gutzman *et al.*, 2008; Grant and Moens, 2010) could prevent high-quality tissue preservation by whole-fish immersion alone. Indeed, the aldehyde fixatives and osmium solution crucial for ultrastructure preservation

appeared to be prevented from crossing a membrane that envelopes the brain in tests of immersion fixation (Figure 3.1a). Additional attempts were made with microwave fixation protocols (Tapia *et al.*, 2012; JoAnn Buchanan, personal communications) that are known to improve penetration of solutions into thick samples, but results were similar to those obtained with immersion fixation.

Larval zebrafish develop a heart and vasculature by 5 days post-fertilization, making vascular perfusion a possibility. Unlike mammals, however, larval zebrafish have a small, two-chamber heart. Injections of tissue processing solutions into the heart were accomplished with a high success rate (Figure 3.1b) and this did deliver fixatives to the brain to some extent. Unfortunately, creating an avenue for outflow is non-trivial, making the amount of solutions that can be injected without substantial swelling too low to accomplish sufficient preservation. Furthermore, red blood cells became locked in place upon fixative injections, thus blocking vessels and preventing solutions from reaching all parts of the brain. Simply severing the tail or clipping a vessel would seem to be options comparable to the right atrium incision made in mammalian *trans*-cardial perfusions, but tests revealed that both result in rapid clotting and re-sealing within ~10 sec. Immersion, microwave-based, and perfusion protocols all resulted in poor quality tissue preservation.

As an alternative approach, a fine dissection was developed that involves removal of the skin and membranes from the dorsum of larval zebrafish while minimizing damage to the brain. Before the dissection, larvae were embedded in low-melt agarose and submerged in a dissection solution containing an anesthetic within a small cell-culture dish. Flow of red blood cells through the vasculature was confirmed by visual inspection before beginning the dissection to ensure health of the larva. A portion of agarose was removed to expose the dorsum from the

Figure 3.1 — Strategies for accessing the larval zebrafish brain with tissue preparation solutions for electron microscopy.

a, Membranes surrounding the brain prevent penetration of aldehyde fixatives and osmium tetroxide. The left side displays brain tissue with poorly preserved ultrastructure. The right side contains cells outside the brain with well-preserved ultrastructure.

b, Injections of fixatives into the heart are possible, but only in limited volumes before pressure build-up and swelling prevent this route of administration from being viable.

c, After dissecting skin and membranes away from the dorsal surface of the brain, aldehyde fixatives and osmium tetroxide are able to enter and better preserve ultrastructure.

d, Diagram of the dissection procedure. The dissection was initiated by puncturing the rhombencephalic ventricle above the hindbrain (red cross) with a sharpened tungsten needle and proceeded with small anterior-directed incisions (red dotted line) along the midline as close to the surface as possible. Larval zebrafish drawing provided by E.A. Naumann and modified by Z.F. Huang Cao.

Scale bars, 1 μm (**a, c**), 50 μm (**b**).

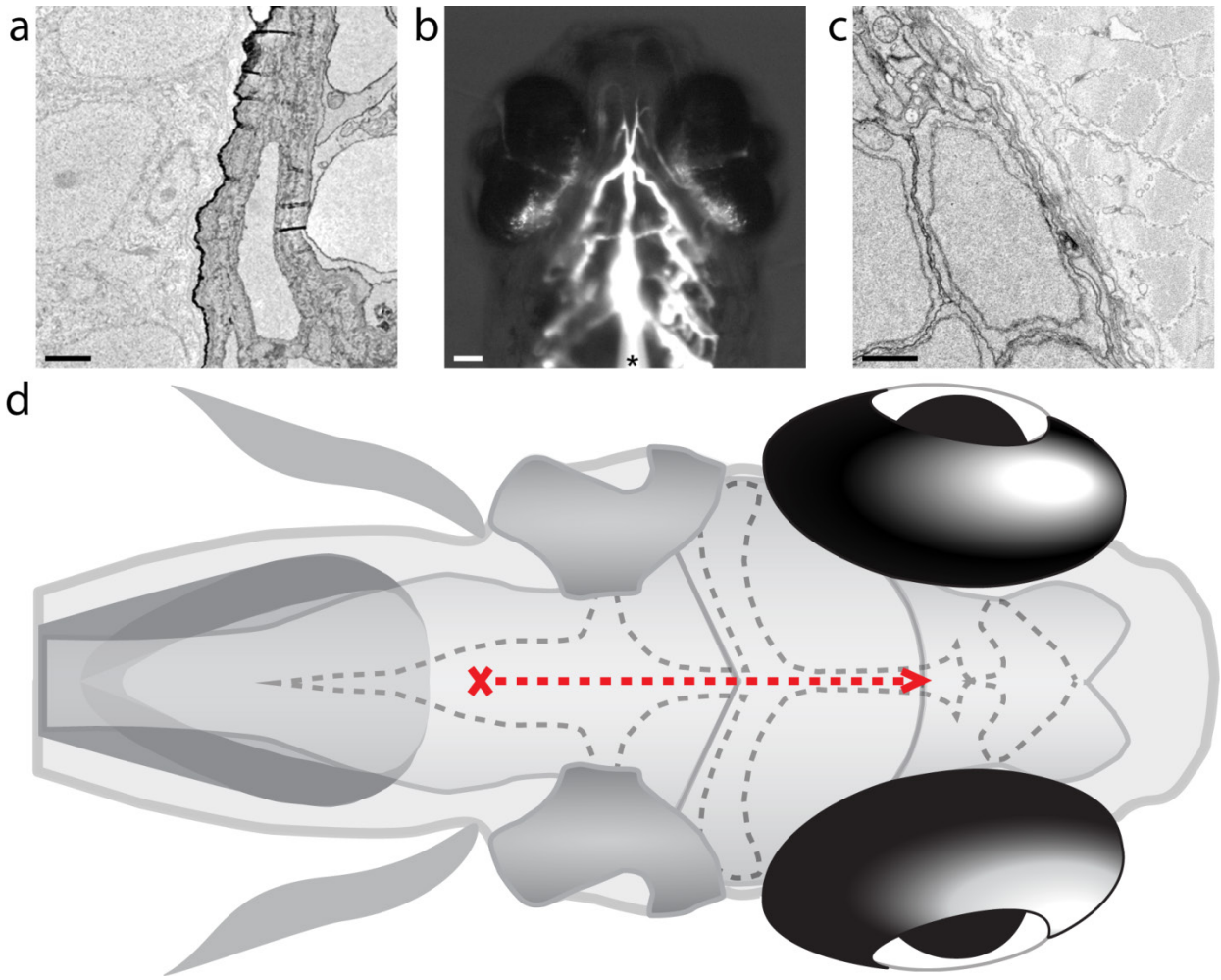

Figure 3.1 (continued)

posterior hindbrain to the anterior optic tectum. The dissection was initiated by puncturing the rhombencephalic ventricle above the hindbrain—the roof of which consists of only a thin epithelial layer (Turner *et al.*, 2012)—with a sharpened tungsten needle and proceeded with small anterior-directed incisions along the midline as close to the surface as possible. The outcome of this procedure was exposed brain from the hindbrain entry site to the middle of the optic tectum (Figure 3.1d). The majority of dissection damage was restricted to proliferating progenitor cells along the midline (Schmidt *et al.*, 2013) that are less likely to have integrated into functional neuronal circuits. Fixatives and other tissue processing reagents gained access to and penetrated throughout the brain tissue (Figure 3.1c) as a result.

Dissections typically took 2–3 min, upon which time a tissue processing protocol previously used for mammalian brain tissue preparation commenced (similar to that used by Bock *et al.*, 2011). The complete cell-culture dish was immersed in aldehyde fixative solution overnight at room temperature (Figure 3.2a). The specimen was then removed in a block of agarose with a scalpel and moved to a microcentrifuge tube for post-fixation in reduced osmium solution (Figure 3.2b) before staining with uranyl acetate (Figure 3.2c). During another wash step, the specimen was freed from the surrounding agarose block and moved to a new tube before being dehydrated with serial dilutions of acetonitrile in double-distilled water (see Section 3.2.3 for details).

Figure 3.2 — Steps involved in preparing larval zebrafish for serial-section electron microscopy.

a, Following fixation, dissection damage can be assessed. Failure to observe cloudy, displaced tissue surrounding the dissection is a good indication of a properly executed dissection.

b, Osmium post-fixation of the larva contained within an excised agarose block results in dense staining of the brain.

c, Uranyl acetate further stains the brain and is particularly visible after dehydration.

d–e, Comparison of a larval zebrafish before and after its caudal and axial fins are removed for placement into the pre-cast embedding mold shown in **f**.

g, Placement of support tissue around the larval zebrafish.

Scale bars, 1 mm (**a**–**g**).

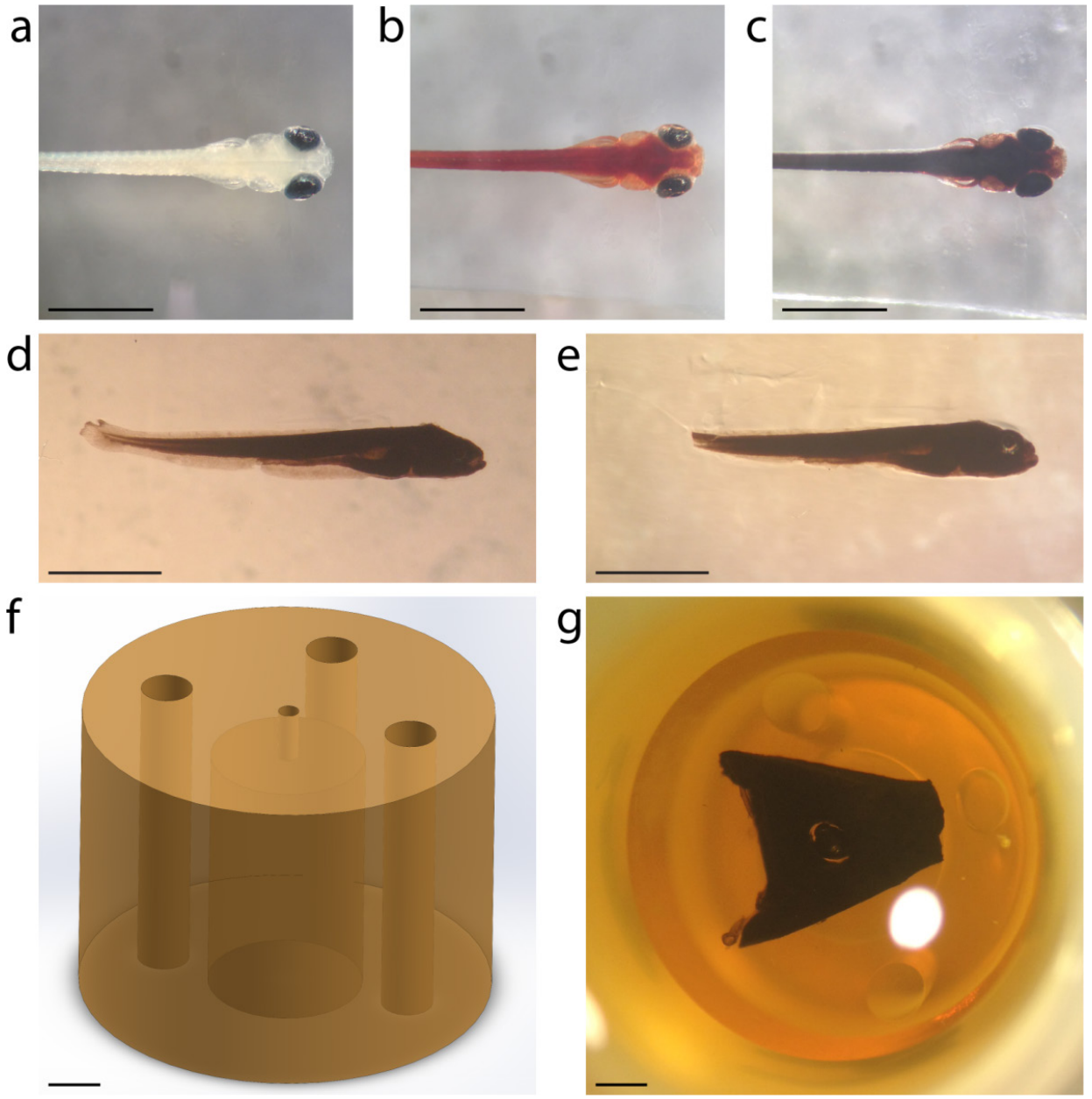

Figure 3.2 (continued)

3.2.2 Embedding for consistent sectioning

Another important aspect of preparing samples for serial-section EM is achieving consistent thin sectioning. To enable sectioning on the order of tens of nanometers for mammalian brain tissue, razor-cut slabs or vibratome sections are typically infiltrated with epoxy resins that polymerize into hard plastic blocks that rarely exceed ~300 μm along the axis of cutting. In larval zebrafish samples, consistent sectioning perpendicular to the long axis (in the direction of forward swimming) is preferable because the majority of axons and dendrites appear to travel along it, and reconstructing the profiles of axons and dendrites cut in cross-section is more straightforward than following those cut tangentially. However, encompassing the complete brain along this dimension for a 5 days post-fertilization larval zebrafish requires ~1 mm of sectioning, or tens of thousands of thin partitions.

During sectioning in test samples, sustained cutting runs over this distance were always complicated by errors and loss. These issues occurred primarily at locations where the composition of the sample changed dramatically, especially at the borders between dissimilar tissues and where the specimen abutted empty epoxy resin. These problems were likely caused by the heterogeneous tissues present in an intact larval zebrafish. Osmium binding occurred at variable densities in dissimilar tissues, which appeared to impose irregular forces on the diamond knife during thin sectioning. For example, an area containing tightly packed membranes—such as the photoreceptor layer of the retina—became heavily stained with osmium, while surrounding areas were not. One way to avoid this would be to extract the complete brain from the rest of the larval zebrafish as is done following perfusions in mammals, but this caused substantial damage to the brain.

Many of the errors produced by testing with commonly used epoxy resins in heterogeneous larval zebrafish tissues involved wrinkling at the interfaces between osmium-rich and osmium-poor regions. These wrinkles almost always extended from interface boundaries into the larval zebrafish brain, obscuring important details that are likely necessary for reconstructing axons and dendrites. Furthermore, abrupt interfaces between tissues and empty resin often caused catastrophic failures where more than 10 sections were lost, gaps too large to follow axons or dendrites across reliably.

Epoxy resins come in several varieties and altering their underlying composition results in a range of physical properties. For example, certain components endow a resin with more hardness, while others provide elasticity. Furthermore, the viscosity of the chosen resin can determine how well it penetrates into a specific type of tissue. Other important considerations include the amount a sample shrinks during polymerization, cutting properties such as the extent to which sections compress, and resin stability during exposure to the electron beam (Finck, 1960).

In an attempt to find an epoxy resin suitable for serial-section EM of the complete larval zebrafish brain, brute-force testing of readily available options was conducted. At least two samples were embedded in each selected resin and tested for sectioning stability. The resins tested included three different hardness formulations for each of the following: Epon 812 (EMbed-812, Electron Microscopy Sciences; TAAB-812, Canemco; LX-112, Ladd Research Industries), Araldite 502-Epon 812 (Electron Microscopy Sciences), Araldite 6005-Epon 812 (Electron Microscopy Sciences), Durcupan (Electron Microscopy Sciences), Spurr's low viscosity (Electron Microscopy Sciences; Ted Pella), Ultra Bed low viscosity (Electron Microscopy Sciences), Hard Plus (Electron Microscopy Sciences), and Luft's low viscosity (Luft,

1973). Of these, Luft's diepoxyoctane-based low viscosity resin performed best, producing the most consistent sectioning with the least losses and fewest observed wrinkling issues. However, substantial problems at the interfaces between empty resin and tissue remained and continued to result in catastrophic events, causing attempts at sectioning even 200 μm through the larval zebrafish to fail.

Reasoning that issues at these interfaces may arise due to abrupt changes in cutting forces, an attempt was next made to provide a more homogeneous sectioning environment by surrounding the specimen not with empty resin but with a support tissue such as mouse liver or cortex. Fins were removed from fixed and stained larvae (Figure 3.2d−e) before infiltration with Luft's low viscosity resin. Following infiltration of the resin, the specimen was placed in the center of a pre-cast resin mold (Figure 3.2f) to ensure stable positioning before a block of similarly processed support tissue with a cylindrical hole punched through it was situated such that it completely surrounded the larva (Figure 3.2g). Liver supports resulted in more reliable sectioning but were too densely stained with osmium and damaged diamond knives rapidly. Cortex supports also produced more consistent sectioning but did not damage diamond knives quickly. Tests consisting of 200 μm cutting sessions with mouse cortex support tissue with a nominal section thickness of 50 nm were successful, with few losses and no catastrophic failures.

3.2.3 Tissue preparation protocol

Detailed tissue preparation and embedding protocols developed in aforementioned experiments are presented in this section for completeness.

3.2.3.1 Materials and reagents

Dissection solution (courtesy of Leung-Hang Ma):

Add each component to double-distilled water to reach the listed final concentration.

64 mM NaCl

2.9 mM KCl

10 mM HEPES

10 mM glucose

164 mM sucrose

1.2 mM $MgCl_2$

2.1 mM $CaCl_2$

Mix until all ingredients are in solution.

Adjust pH to 7.5 with 0.2 N NaOH.

Add double-distilled water to reach the desired final volume.

Use with 0.02% (w/v) tricaine mesylate (MS-222) for anesthesia.

Mixed aldehyde fixative solution:

Add each component to reach the listed final concentration.

2.0% paraformaldehyde (from 16% stock)

2.5% glutaraldehyde (from 25% stock)

0.08 M Sorensen's phosphate buffer (from 0.2M, pH 7.4 stock)

Add double-distilled water to reach the desired final volume.

Glutaraldehyde fixative solution:

Add each component to reach the listed final concentration.

3% glutaraldehyde (from 25% stock)

0.08 M Sorensen's phosphate buffer (from 0.2M, pH 7.4 stock)

Add double-distilled water to reach the desired final volume.

Reduced osmium solution:

Make fresh 3% (w/v) potassium ferricyanide in double-distilled water.

Add and equal volume of cold (+4°C) 2% aqueous osmium tetroxide drop-wise into cold 3% potassium ferricyanide.

The resulting solution contains 1% osmium tetroxide and 1.5% potassium ferricyanide in double-distilled water.

Keep cold until use.

Maleate buffer stock solution:

Add each component to 25 mL of double-distilled water.

2.32 g maleic acid

20 mL 1 N NaOH

Adjust pH to 6.0 with 0.2 N NaOH.

Add double-distilled water to reach 100 mL final volume.

The resulting solution contains 0.2 M maleate buffer and is pH 6.0.

Maleate buffer wash solution:

Add each component to 50 mL of double-distilled water.

25 mL 0.2 M maleate buffer stock, pH 6.0

4.2 mL 0.2 N NaOH

Adjust pH to 5.15 with 0.2 N NaOH.

Add double-distilled water to reach 100 mL final volume.

The resulting solution contains 0.05M maleate buffer and is pH 5.15.

Uranyl acetate solution:

Add each component to 50 mL of double-distilled water.

1 g uranyl acetate

25 mL 0.2 M maleate buffer stock, pH 6.0

Mix with a stir bar at room temperature for several hours or sonicate until uranyl acetate is in solution.

Adjust pH to 5.15 with 0.2 N NaOH.

Add double-distilled water to reach 100 mL final volume.

Pass through 0.2 μm filter before use.

The resulting solution contains 1% uranyl acetate and 0.05 M maleate buffer and is pH 5.15.

Luft's low viscosity epoxy resin:

Mix the specified volume of each component thoroughly into a 50 mL tube.

18 mL diepoxyoctane (DEO)

32 mL nonenyl succinic anhydride (NSA)

Add 0.75 mL DMP-30 epoxy polymerization accelerant and mix thoroughly.

Allow any visible air bubbles to dissipate before use.

3.2.3.2 Protocol

Day 1 — Fixation

1. Immobilize 5–7 days post-fertilization larval zebrafish with α-bungarotoxin.
2. Mount specimen in 1.5–2.0% low-melt agarose in a small dish.
3. Perform activity mapping experiments (optional).
4. Anesthetize by adding dissection solution containing tricaine.
5. Perform dissection with a sharpened tungsten needle (Figure 3.1d).
6. As quickly as possible after dissection, immerse the entire dish in a chamber containing mixed aldehyde fixative solution (Figure 3.2a).
7. Incubate for 2–4 hr at room temperature.
8. Wash with 0.08M Sorensen's phosphate buffer (3 × 10 min).
9. Continue fixation in glutaraldehyde fixative solution.
10. Incubate overnight at room temperature.

Day 2 — Post-fixation and staining

11. Wash with 0.08M Sorensen's phosphate buffer (3 × 10 min).

12. Wash with double-distilled water (3 × 10 min).
13. Gently remove block of agarose containing specimen with scalpel, move to tube.
14. Post-fix with reduced osmium solution for 2 hr at room temperature (Figure 3.2b).

    For support tissue, post-fix for 12–24 hr.
15. Wash with double-distilled water (3 × 10 min).
16. Move specimen to new tube with transfer pipette.
17. Wash with maleate wash solution (3 × 10 min).
18. Stain with uranyl acetate solution (Figure 3.2c).
19. Incubate overnight at room temperature.

Day 3 — Dehydration and infiltration

20. Wash with maleate wash solution (3 × 10 min).
21. Gently remove specimen from agarose with eyelashes and toothpicks.
22. Carefully remove caudal and axial fins with a fine scalpel.
23. Move specimen to new tube with transfer pipette.
24. Wash with double-distilled water (3 × 10 min).
25. Dehydrate with serial acetonitrile dilutions in double-distilled water (10 min each).

    25%, 50%, 70%, 70%, 80%, 90%, 95%, 100%, 100%, 100%
26. Infiltrate with serial Luft's low viscosity resin dilutions in acetonitrile (1 hr each).

    25%, 50%, 75%, 100%

    Be cautious when handling Luft's low viscosity resin, diepoxyoctane is very toxic and volatile.
27. Infiltrate overnight with 100% Luft's low viscosity on a rotating platform.

Day 4 — Infiltration and embedding

28. Continue infiltration with fresh 100% Luft's low viscosity on a rotating platform for 3 hr.
29. Position pre-cast placement mold in a BEEM embedding capsule containing Luft's low viscosity resin while avoiding creation of air bubbles.
30. Add sample in resin to the BEEM capsule using a transfer pipette.
31. Gently position the sample into the placement mold using eyelashes.
32. Place similarly processed support tissue around specimen.
33. Embed by hardening resin at 60°C for 2–3 days.

3.3 Whole-brain sectioning and imaging

With protocols and methods in place for tissue processing and consistent sectioning of nearly intact larval zebrafish, application at the whole-brain scale was targeted. Automated tape-collecting ultramicrotomes consist of a customized addition to commercial Leica Microsystems ultramicrotomes (Hayworth *et al.*, 2006; Schalek *et al.*, 2011; Hayworth *et al.*, 2014). In its original form, the automated tape-collecting device was capable of holding reels of 50 µm-thick Kapton® tape lengths of ~45 m. A typical section spacing of ~6 mm was required for using the support tissue system described previously, leading to a maximum of ~7,500 collected sections onto a reel. A sectioning thickness of ~133 nm would be needed to capture sections containing the entire larval zebrafish brain with these limitations, but the gaps between surfaces at this thickness are too large to reconstruct many small axons and dendrites (Briggman and Bock, 2012). To overcome this restriction, a modified automated tape-collecting ultramicrotome was built to hold larger reels that accommodate ~98 m of tape (Figure 3.3). This system enabled collection of ~19,500 sections, thus enabling sectioning at thicknesses of 50–60 nm throughout the complete brain.

The brains of two specimens were sectioned with this modified automated tape-collecting ultramicrotome setup. The first sample was sectioned into ~15,000 × ~50 nm-thick sections, but was not pursued further because the series missed a significant portion of the hindbrain. Partitioning of the second, more complete sample involved cutting 18,207 × ~60 nm-thick sections spanning ~95 m of tape. This tape was then cut into fragments and adhered to 80 silicon wafers that each served as a stage for imaging within a scanning EM (Figure 3.4). Each wafer carried ~225 sections.

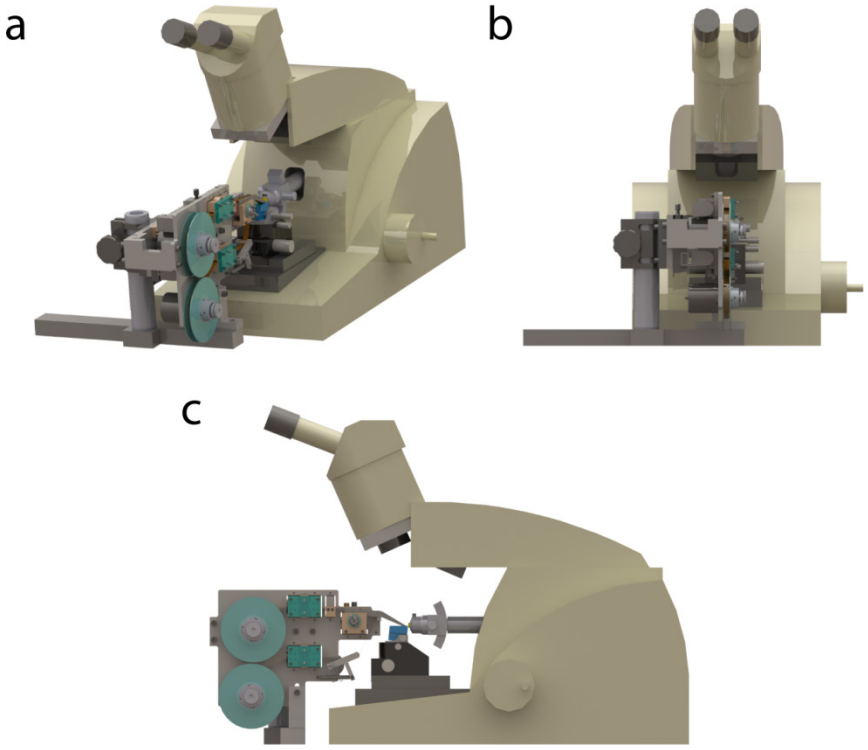

Figure 3.3 — Modified automated tape-collecting ultramicrotome. In order to collect ~20,000 serial sections, an automated tape-collecting ultramicrotome was modified to house larger reels of tape. The altered design is illustrated here in (**a**) perspective, (**b**) lateral, and (**c**) front views. The ultramicrotome attached to the tape-collecting device is a Leica EM UC6. Modified from drawings produced by K.J. Hayworth.

Figure 3.4 — Library of thin sections spanning a complete brain.

a, Tape fragments containing 18,207 × ~60 nm-thick serial sections that span a complete larval zebrafish brain stored on 80 silicon wafers that serve as an imaging stage.

b, View of a single wafer (from box in **a**).

Scale bar, 1 cm.

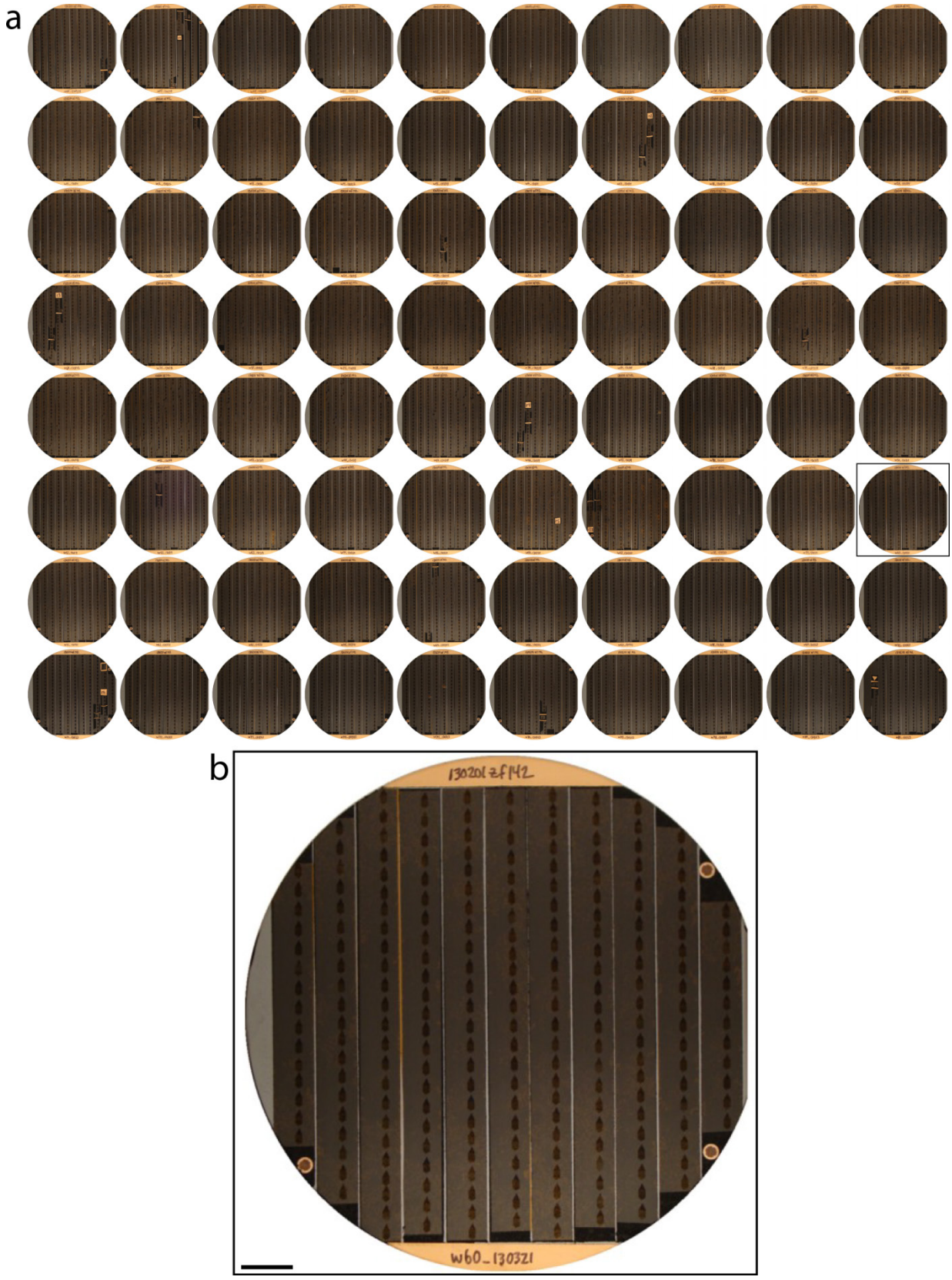

Figure 3.4 (continued)

Broad scanning EM overview images were acquired at a resolution of ~750 nm×px^{-1} to survey all sections in this series (Figure 3.5a, Figure 3.7a). This process required 5.4 days of imaging, resulting in a stack of 17,963 images spanning 1.02×10^{10} μm^3, consisting of 3.01×10^{11} voxels of 8-bit depth, and occupying 252 gigabytes of computer storage. In total, the anterior quarter of the larval zebrafish (Figure 3.5b–d) was partitioned into 17,963 × ~60 nm-thick sections collected from 18,207 attempted. From this series, 244 sections were lost (1.34%; Figure 3.5e top) and 283 contained only partial regions of the tissue (1.55%; Figure 3.5e middle). Many partial sections still contained a substantial portion of the brain, so these were classified further as: minor for very small losses, moderate for missing portions of half the brain or spinal cord area, or severe for missing portions greater than half the brain or spinal cord area categories (Figure 3.6). There were no adjacent losses and 5 instances of adjacent combinations of lost-partial or partial-partial sections (Fig. 3.5e bottom). From this low-resolution data, it was confirmed that this sectioning approach enabled stable serial sectioning through a millimeter-long region spanning from myotome 7 to the anterior-most larval zebrafish structures—encompassing part of the spinal cord (Ma *et al.*, 2009) and the entire brain (Figure 3.5d).

Selected sub-regions from within the collected volume were next targeted to capture areas of interest at higher resolutions from the persisting sections using a multi-scale imaging approach (Hayworth *et al.*, 2014). With these regions of interest translated into stage coordinates, co-registered section overview images were used to semi-automatically target subsequent rounds of imaging (Figure 3.7a). All subsequent scanning EM was aided by technical assistance from George S. Plummer. To first develop a clearer view of what was contained within the series, isotropic EM imaging—with lateral resolution matching the nominal sectioning thickness—was

Figure 3.5 — Whole-brain serial sectioning of larval zebrafish for electron microscopy.

a, Plastic resin-embedded samples are cut into thin sections with a diamond knife and collected by an automated tape-collecting ultramicrotome. Overview micrographs were acquired from a collection of 18,207 × ~60 nm-thick transverse serial sections that span 1.09 mm. Embedding the larval zebrafish in a support tissue was found to stabilize sectioning.

b, Volume rendering from overview images reveal the portion of the larval zebrafish collected.

c, Volume rendering with planes corresponding to the section (green) and reslice views (from **d**).

d, Reslice planes through all overview images show the structures contained within the series and illustrate the sectioning plane relative to the horizontal (top) and sagittal (bottom) body planes. Lines depict the relative position of each reslice plane.

e, Histograms of the percent of lost, partial (missing any larval zebrafish tissue), or adjacent (lost-partial or partial-partial) events per bin of 63 sections throughout the series. In total, 244 (1.34%) sections were lost and 283 (1.55%) were partial. No two adjacent sections were lost.

Scale bars, 250 μm (**a**, **d**).

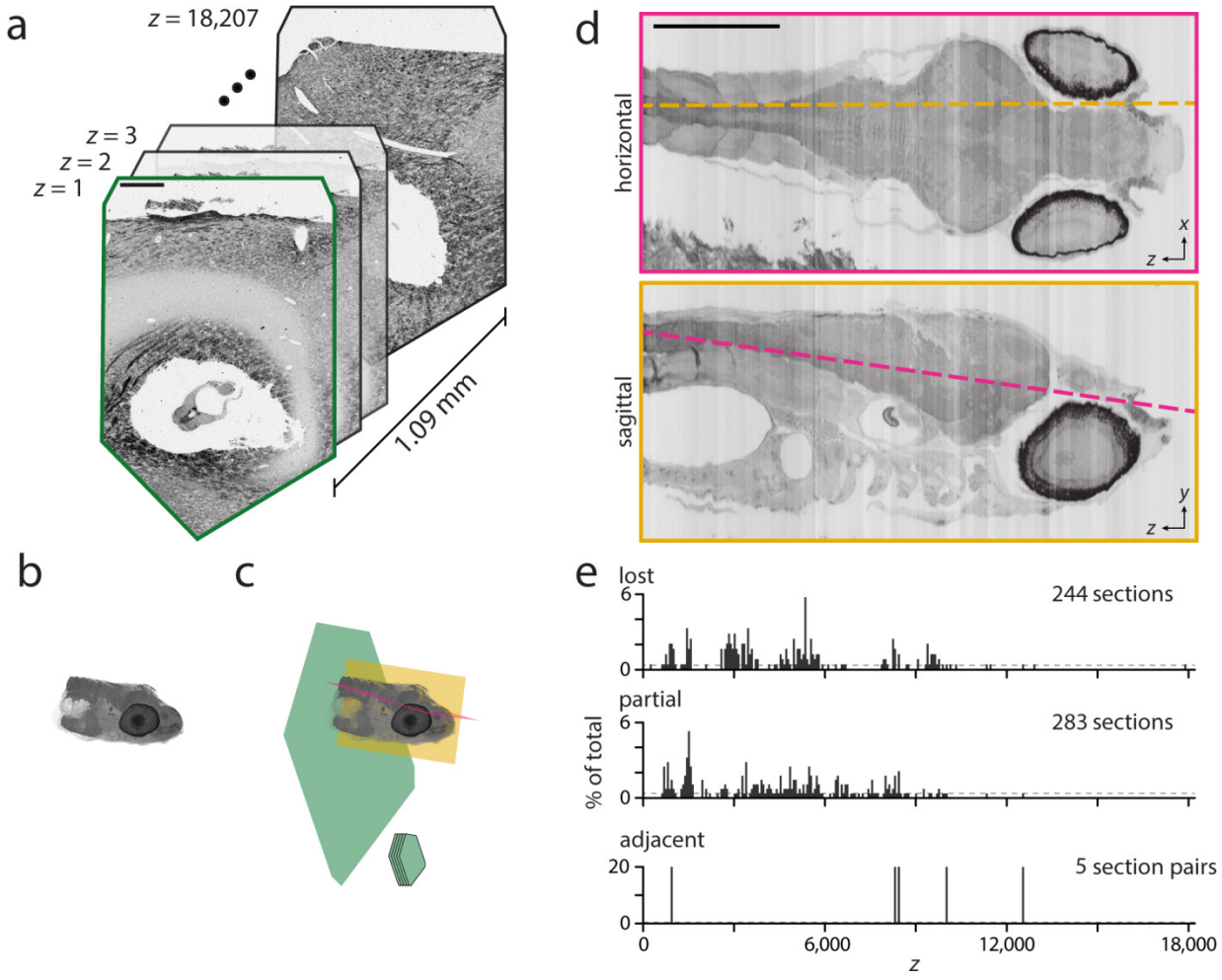

Figure 3.5 (continued)

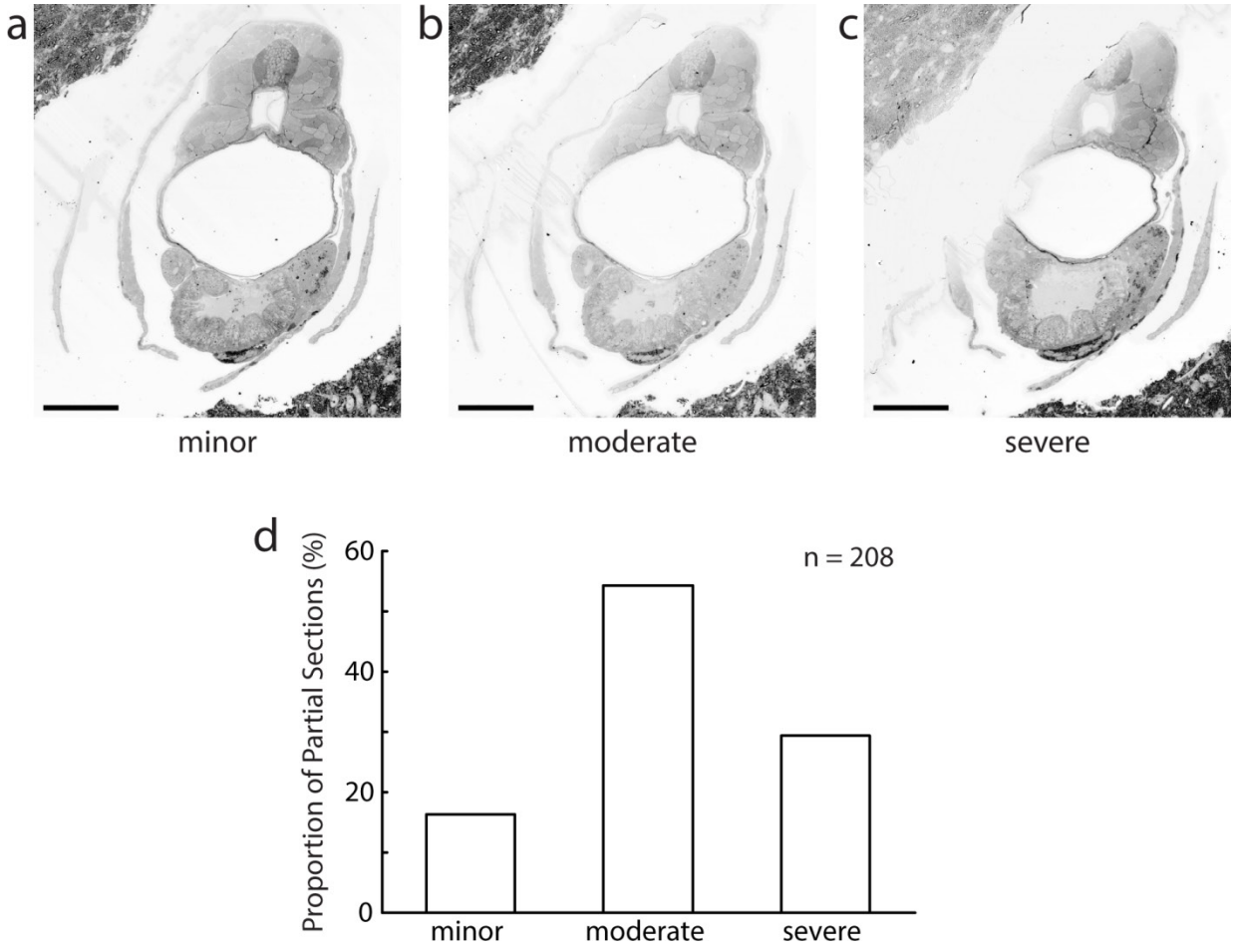

Figure 3.6 — Partial sections were classified as any section with larval zebrafish tissue missing. These were further classified as minor (**a**) for very small losses, moderate (**b**) for missing portions of half the brain or spinal cord area, or severe (**c**) for missing portions greater than half the brain or spinal cord area.

d, Classification of the 208 partial sections contained within the 16,000 anterior-most sections. Scale bars, 100 μm (**a**–**c**).

Figure 3.7 — Targeted multi-scale scanning electron microscopy of the larval zebrafish brain.

a, Coarsely aligned section overview micrographs enable targeting for subsequent imaging at higher resolution (colored outlines indicate regions targeted in **b** and **c**).

b, Isotropic imaging of transverse sections with lateral resolution matching the nominal thickness provides access to large features including cell nuclei (as shown in **b′**).

c, Imaging of the brain at 20 nm×px^{-1} lateral resolution reveals myelinated axons (**c′** top left), fasciculated neuronal processes (**c′** top right), and large dendrites (**c′** bottom).

d, High-resolution imaging unveils individual axon and dendrite contours and permits identification of synapses (orange arrows).

Scale bars, 250 µm (**a**), 50 µm (**b**), 25 µm (**c**), 10 µm (**b′**), 2 µm (**c′**), 500 nm (**d**).

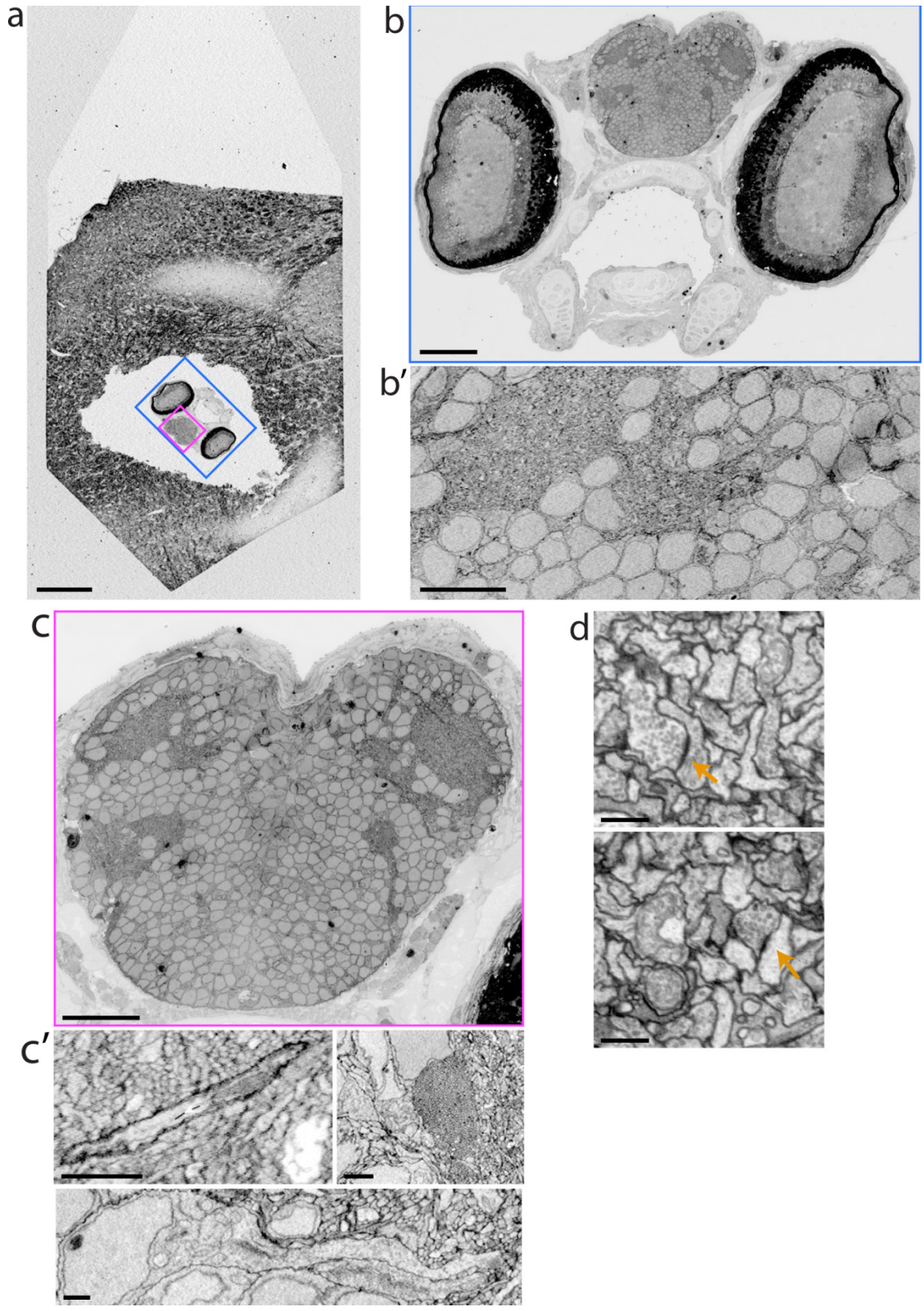

Figure 3.7 (continued)

performed of the larval zebrafish body cross-section contained in each of the anterior-most 16,000 sections (Figure 3.7b).

This image volume contained the anterior quarter of the larval zebrafish including the brain, sensory organs (e.g., eyes, ears, olfactory pits), and many other tissues at a resolution of 60 nm×px^{-1}, or ~500 times that afforded by light after considering section thickness. It spans 2.28×10^8 μm^3, consists of 1.12×10^{12} voxels of 16-bit depth, occupies 2.1 terabytes (TB), and took 97 days to acquire. In this data, cell nuclei (Figure 3.7b′) can be readily identified and large-caliber myelinated axons traveling outside the brain can be followed. To further resolve fine neuronal structures, a third round of imaging at 20 nm×px^{-1} was conducted, resulting in a high-resolution atlas of the brain over 12,546 sections (Figure 3.7c). This image volume spans 5.49×10^7 μm^3, consists of 2.36×10^{12} voxels at 16-bit depth, occupies 4.4 TB, and took 100 days to acquire. With this data, it is possible to identify and reconstruct bulk, inter-areal connectivity throughout the larval zebrafish brain in the form of myelinated axons and co-fasciculated bundles of axons or dendrites (Figure 3.7c′).

By co-registering the 60 nm×px^{-1} and 20 nm×px^{-1} image volumes, it is also possible to follow large-caliber myelinated inputs from sensory organs into the brain and from motor neurons in the spinal cord to muscles. Initial intra- and inter-section image alignments were performed with Fiji TrakEM2 alignment plug-ins (Saalfeld *et al.*, 2010; Schindelin *et al.*, 2012). More sophisticated, non-linear image registration is ongoing in collaboration with Art W. Wetzel of the Pittsburgh Supercomputing Center.

The complete brain dataset acquired at 20 nm×px^{-1} is very unlikely to be sufficient for reconstructing all axons and dendrites or the synapses that form the connections between them. However, the multi-resolution imaging technique enables targeted revisiting to locations

contained within the library of ultrathin sections for re-acquisition at higher resolutions. When this imaging is performed, it is possible to identify synapses and clearly separate most axon and dendrite profiles (Figure 3.7d).

3.4 Correspondence with activity mapping data

The whole-brain serial-section EM dataset was acquired from a *Tg(elavl3:GCaMP5G)a4598* larval zebrafish (Ahrens *et al.*, 2012) with genotype *elavl3*:GCaMP5G$^{+/+}$; nacre (*mitfa*$^{-/-}$). Using this line—which exhibits nearly pan-neuronal expression of the calcium indicator GCaMP5G (Akerboom *et al.*, 2012) and increased transparency due to the nacre mutation (White *et al.*, 2008)—permitted testing of the ability to preserve individual neuron identity across functional and *post hoc* structural imaging modalities. Because activity mapping is conducted at roughly cellular resolution, accomplishing this requires correspondence of neuronal nuclei positions contained within the EM dataset to those identified with whole-brain imaging by light.

In vivo two-photon image stacks were collected in collaboration with Ruben Portugues and Isaac H. Bianco prior to dissection and tissue processing in order to capture a snapshot of anatomy consistent with that obtained during activity mapping experiments (Figure 3.8a,b,c). After acquisition and initial inter-section alignment, the EM dataset was aligned by three-dimensional affine registration to the *in vivo* fluorescence dataset through manual placement of fiducial points with software previously created by Hunter L. Elliot. The transformed EM dataset (Figure 3.8a′,b′,c′) facilitated matching of nuclei positions, making it possible to identify the same neurons across imaging modalities in most observed cases (Figure 3.8c″). Individual nuclei in low-fluorescence areas were difficult to discern, but were generally positioned along midline in areas that consist primarily of progenitor cells (Schmidt *et al.*, 2013), which are less

likely to play a functional role in neuronal circuits. The ability to correspond neuron identity across imaging modalities allows, in principle, the integration of rich neuronal activity maps with subsequent whole-brain structural interrogation targeted to functionally characterized neurons.

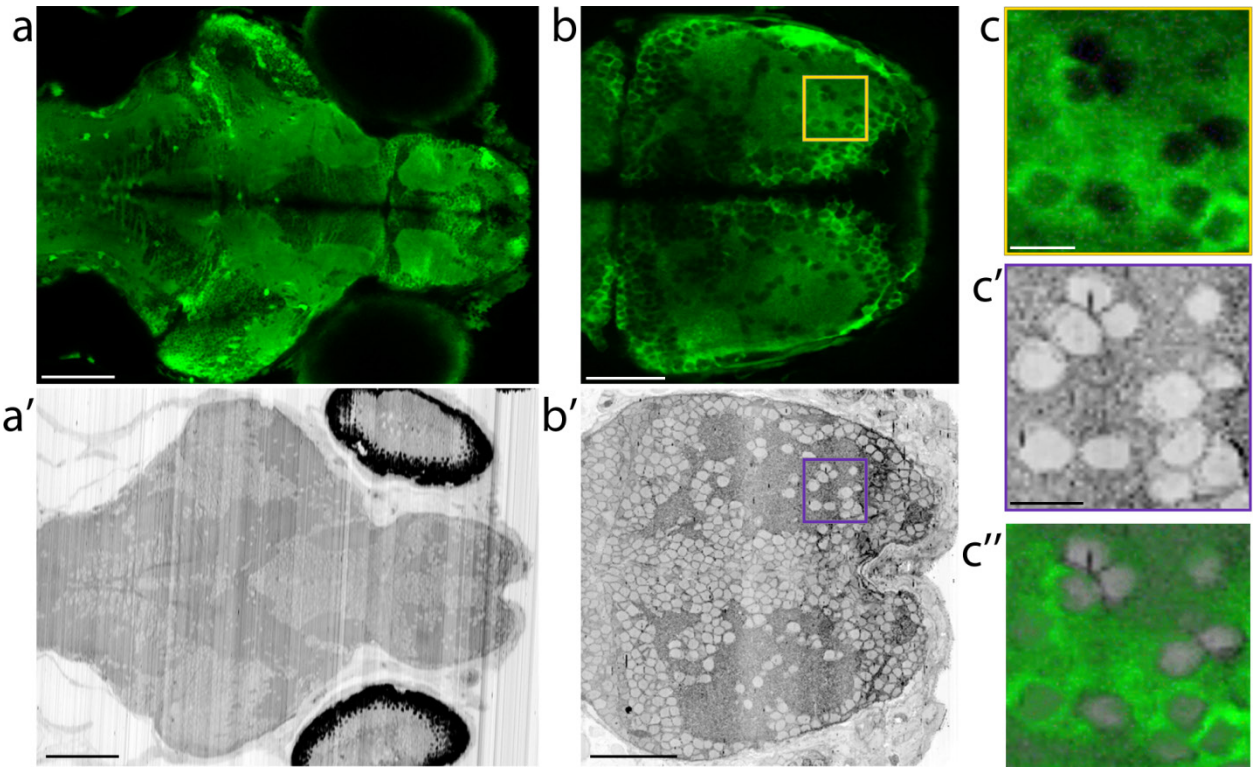

Figure 3.8 — Correspondence between *in vivo* fluorescence and electron microscopy datasets.

a, Single slice from whole-brain two-photon imaging of a transgenic zebrafish line expressing GCaMP5G in almost every neuron. This specimen was subsequently prepared for electron microscopy.

a′, Resliced horizontal plane of isotropic electron micrograph stacks near the same dorsoventral level as **a**.

b–**b′**, Corresponding features in the telencephalon found by iterative manual affine registration of electron microscopy to fluorescence data. The areas scanned in **c** and **c′** are indicated by boxes in **b** and **b′**, respectively.

c–**c′,** Example case illustrating the preservation of neuron identity across imaging modalities. **c″**, Overlay of **c** and **c′**.

Scale bars, 100 µm (**a**–**a′**), 50 µm (**b**–**b′**), 10 µm (**c**–**c′**).

3.5 Neuron reconstruction and data analysis

The high-resolution whole-brain larval zebrafish atlas acquired at 20 nm×px^{-1} lateral resolution should be sufficient for reconstruction of many neuronal structures, particularly myelinated processes (Figure 3.7c′). Furthermore, annotating these structures should provide a map of inter-areal (region-to-region) connections, providing insights into the main highways of communication in the larval zebrafish brain.

In order to test if reconstructing myelinated structures was possible in this dataset, it was first necessary to align all the raw electron micrographs into a continuous series. While the semi-automatic targeting of high-resolution acquisition from coarsely aligned section overview images reduces the burden of co-registering adjacent images, stage inaccuracies and differential compression of sections during the cutting process result in substantial differences that must be corrected. The Fiji software package's TrakEM2 alignment plug-ins (Saalfeld *et al.*, 2010; Schindelin *et al.*, 2012) were used to overcome the majority of these issues. An initial round of intra-section alignment was performed to register each 20 nm×px^{-1}, brain-only image to its corresponding 60 nm×px^{-1} complete larval zebrafish cross-section image. Subsequently, the images within each section were locked relative to one another. One round of rigid inter-section alignment was then completed before a final affine inter-section alignment. The resulting aligned image volume was flattened and exported such that the regions within each section containing only 60 nm×px^{-1} lateral resolution data were up-sampled to 20 nm×px^{-1}. This up-sampling step increases the computer storage required for the final dataset output but was required for compatibility with reconstruction software. Software changes have since been made to prevent this from being required for future datasets.

The intra- and inter-section aligned dataset was next imported into the Collaborative Annotation Toolkit for Massive Amounts of Image Data, or CATMAID (Saalfeld *et al.*, 2009), a web-based software tool that permits simultaneous manual annotation of large image datasets by multiple users. Myelinated structures throughout the brain were identified by the characteristic membrane density surrounding the axon or dendrite profile (Figure 3.7c′). To begin reconstruction, a CATMAID treenode object was created for each identified myelinated structure. Each such "seed" object consisted of a partial annotation of the myelinated structure generated by placing a single node in the center of the axon or dendrite membrane contour contained within each of 10–20 adjacent sections. Each seed object was then assigned to a single annotator for more complete reconstruction of the neuron's morphology. This work was aided by technical help from several annotators: C.S. Elkhill, G.S. Plummer, R.J. Plummer, I. Odstrcil, M.D. Petkova, P.I. Petkova, P. Lewis, K. Runci, A. Haddad, A. Coda, A. Cohen, and F. Camacho Garcia.

The resulting annotations reveal that reconstruction of axons and dendrites that traverse more than 550 μm (spanning more than 9100 sections) are possible in this dataset (Figure 3.9a–b). Many of the reconstructed neurons extended from the brain out to sensory structures such as lateral line neuromasts. Motor neurons in the spinal cord that were identifiable by morphology alone were also found extending myelinated axons to innervate muscles. For each neuron, the locations of the nucleus and gaps in myelination were also annotated whenever possible. Of 300 seeded myelinated structures, 265 were traced until they became unmyelinated for more than 50 sections. Additional elaboration of the remaining seeds, further surveying and seed placement at intervals of 50 sections, and review of reconstructed neurons by a second annotator are currently under way. The resulting annotations will form a map of the myelinated inter-areal (region-to-

region) connections throughout the larval zebrafish brain that can be further analyzed to identify patterns of myelination.

This dataset will also permit identification of neuronal nuclei for accurate neuron counts, size approximation, and region-by-region distribution analyses. Work in collaboration with W.-K. Jeong and Q.T. Minh resulted in the development of an algorithm for automatic segmentation of nuclei throughout the brain, which will be used for these studies (Figure 3.9c).

Figure 3.9 — Extraction of features from the whole-brain serial-section EM dataset.

a, Horizontal reslice showing the orientation of rendering in **b**.

b, Manually reconstructed myelinated axons throughout the brain and body.

c, Initial testing from a region of the telencephalon reveals that neuronal nuclei can be automatically segmented (left). Distinct nuclei are represented by different colors. Neuropil regions are rendered transparent, therefore appearing white here. Example for a small volume depicting the segmentation process (right). Images in **c** produced by Q.T. Minh.

Scale bar, 250 μm (**a**).

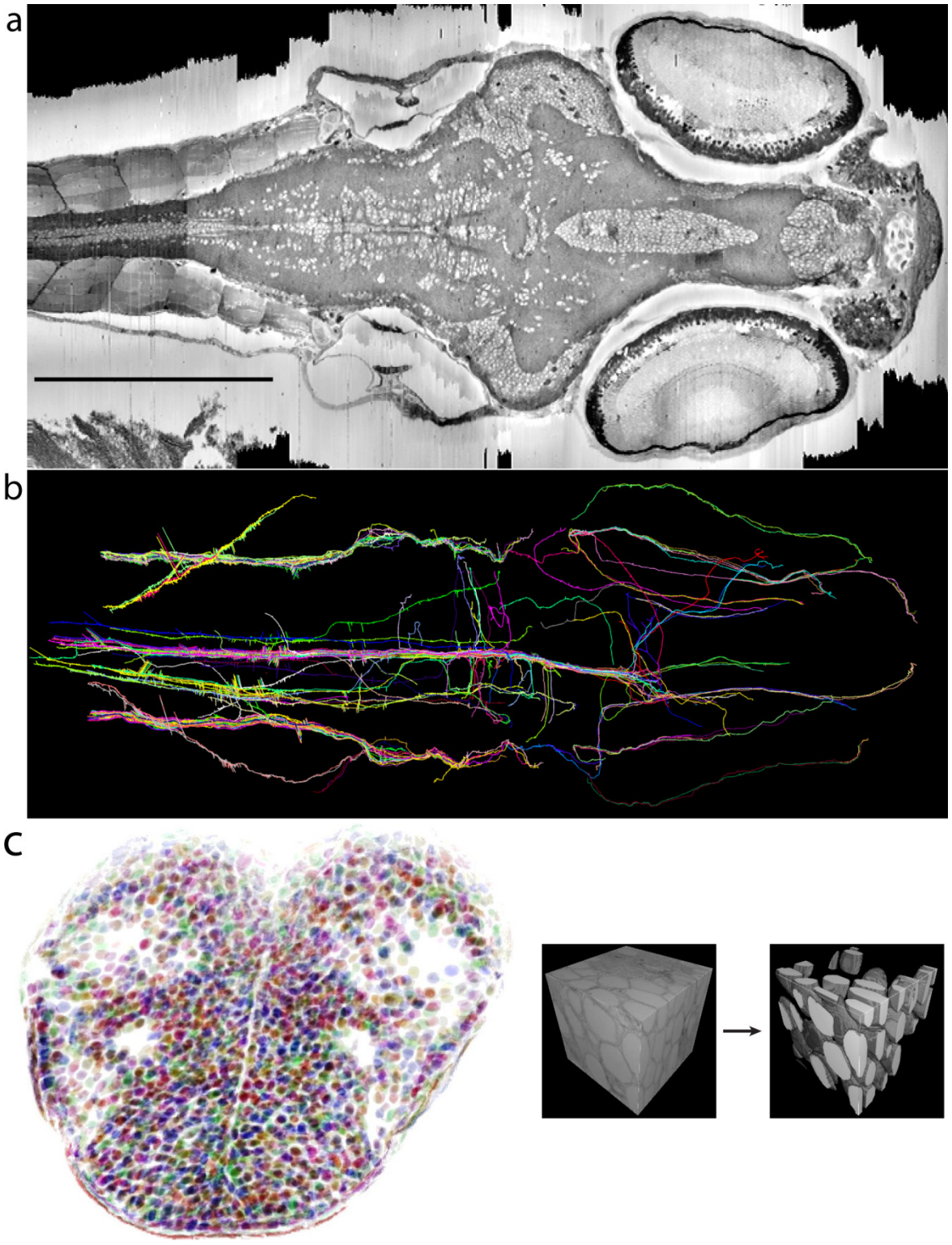

Figure 3.9 (continued)

3.6 Conclusions

The results presented in this chapter demonstrate the feasibility of whole-brain serial-section EM in larval zebrafish and illustrate the utility of multi-scale imaging for optimizing imaging time and data storage expenses. This approach opens up the possibility of whole-brain imaging at moderate resolutions with targeted or random-access re-imaging at higher resolutions only in areas where additional reconstruction or confirmation of synapses is needed. Continued development of EM technologies will hasten this re-imaging process and permit whole-brain serial-section EM studies in a fraction of the time required to collect the data presented here. Additionally, this chapter revealed that EM datasets can be combined with activity mapping datasets to combine functional and structural information about most neuronal circuits in the larval zebrafish brain.

Notably, these datasets are not limited to analyses of the nervous system and can easily be extended to examine the structure of other organ systems. The dataset described here also includes musculoskeletal, cardiac, intestinal, pancreatic tissues, and more. The data can thus be used as an anterior larval zebrafish reference atlas and is freely available for study by the broader scientific community. One such group has already used this atlas to identify a new type of cellular junction in the endolymphatic sac that regulates pressure in the inner ear, a study that has been submitted for publication (Swinburne *et al.*, submitted).

Chapter 4

Discussion

4.1 Overview

This dissertation demonstrates that it is possible to perform whole-brain calcium imaging and *post hoc* whole-brain serial-section electron microscopy (EM) in larval zebrafish. Furthermore, it shows that these datasets can be combined toward examining the relationships between neuronal circuit structure and function. The methodological framework developed here provides an avenue for extensive analyses of neuronal circuits that span a complete vertebrate brain. However, the experience of producing the first proof-of-concept datasets has exposed several improvements that could be made to facilitate this work. This chapter describes the identified shortcomings and suggests alternative approaches to overcome them in future experiments.

4.2 Method shortcomings and potential improvements

4.2.1 Model organism choice

Several aforementioned properties of the larval zebrafish make it an excellent model organism for examining neuronal circuit structure and function (see Section 1.4). However, it is important to consider that most of the traits that make this model organism so attractive—including transparency, small size, and ease of nearly pan-neuronal expression—have been exploited primarily during the 5 to 7 days post-fertilization window, a sustained period of rapid development. Although the behavioral repertoire and ability to learn expand as zebrafish age (Lee *et al.*, 2010; Hinz *et al.*, 2013), most common promoters that drive expression in practically all neurons wane beyond 7 days post-fertilization, thereby limiting past calcium imaging efforts. New strategies are being developed to sustain robust expression out as far as 14 days post-fertilization (Kim *et al.*, 2014), now enabling calcium imaging in older larval zebrafish. It will

be important to consider the trade-offs between calcium reporter expression, translucence, and brain size with respect to neuronal circuits and behaviors of interest in future studies whole-brain structural and functional studies.

The stage of development may also have profound effects on the outcome of whole-brain serial-section EM experiments. Because apparently little serial-section EM has been performed in larval zebrafish, it is difficult to assess the quality of tissue preservation. Holding data obtained from larval zebrafish to the standards of relatively stable adult mammalian tissues is tempting, but potentially misleading. Some artifacts of poor fixation quality are likely to appear similar to naturally retracting and blebbing neuronal structures that are undergoing developmental refinement. The appearance of broken membranes across entire datasets should still raise concern, but degradation in a small subset of axon or dendrite profiles could be caused either by damage to neurons during tissue preparation or to natural processes under way in this rapidly developing animal. Determining the standards for tissue preservation in larval zebrafish EM experiments will require more extensive study.

4.2.2 Calcium imaging and transgenic zebrafish lines

Activity mapping experiments have progressed rapidly in larval zebrafish, largely due to the fast generation of transgenic lines. However, the current standard of qualitatively assessing "pan-neuronal" expression by surveying anatomical image stacks (as performed in Chapter 2) is insufficient. While it is understandable that investigators want to move on to interesting neuroscience questions as quickly as possible once a new transgenic line is available, comparing the distribution of expression across lines by cross-registration of fluorescence image stacks with different promoters would improve our knowledge of which neurons are missing from current

calcium imaging experiments. Take for example the well-studied Mauthner neuron that is involved in escape behaviors, which does not appear to be labeled by the *elavl3 cis*-regulatory elements. Furthermore, these experiments would make it possible to compare across transgenic lines expressing the same indicator that likely have different integration sites. For example, other labs have now produced transgenic lines with expression similar to the *Tg(elavl3:GCaMP6f)a12200* line (Vladimirov *et al.*, 2014), and comparing them would help identify and explain any differences in activity mapping results. Recent studies have made substantial progress in cross-registration of brains from the same zebrafish lines to compare activity patterns across experiments (Portugues *et al.*, 2014). New efforts to apply these methods to compare across lines (Randlett *et al.*, submitted) should increase reliability and confidence in the results from whole-brain calcium imaging studies.

Additionally, cytosolic expression of calcium indicators, as present in the *Tg(elavl3:GCaMP6f)a12200* line described in Chapter 2, frequently makes it difficult to assign calcium signals to a single neuron because they are often tightly packed in clusters with overlapping fluorescence signal (see Figure 2.3c or Figure 2.6c). New transgenic lines are now being produced with nuclear-restricted expression of calcium indicators such as GCaMP3 (Kim *et al.*, 2014) and GCaMP6 (Vladimirov *et al.*, 2014), which results in expression similar to that found in the *Tg(elavl3:H2B-mRFP)a9486* line. Additional characterization of how well the nuclear-restricted reporters track activity will be important, particularly for the nuclear-restricted GCaMP6 indicator lines, but initial results with truly single neuron-resolution analyses from these lines are promising.

4.2.3 Serial-section electron microscopy

The methods for producing serial sections described in Chapter 3 makes it possible to extract ultrastructural details from the entire larval zebrafish brain. Merging this approach with multi-scale imaging decreases the cost and time burdens of acquiring whole-brain EM datasets. However, multiple improvements will be important for enhancing complete neuronal circuit examination using this preparation. These include causing less damage with dissections, preserving tissue better, decreasing section thickness, faster imaging, and specific labeling.

The dissection developed to provide fixatives access to the brain results in midline-restricted damage to the dorsal surface of the brain. Though most of the cells in this region are likely to be progenitors, this procedure should be refined to minimize damage. One alternative would be to tear skin away from muscle over the spinal cord and pull it anterior to expose the brain (Fabian Svara, personal communication). This would avoid prodding the skin atop the brain with a sharpened tungsten needle, which can accidentally probe too deep during the dissection process. It is unclear how well this alternative technique will be able to preserve sensory structures outside the brain and how much distortion of the brain may result, but it is important to consider and attempt as many alternative dissection protocols as possible to find the one that causes the least damage.

As described in Section 4.2.1, it is difficult to know exactly how well-preserved larval zebrafish brain ultrastructure will compare to well-preserved mammalian brain. However, it is unlikely that the protocol used here, which was created for use with mammalian brain tissues, is ideal. This is most evident in the tortuous appearance of membranes when visualized at high resolution (see Figure 3.7d). While reconstructions of individual axons and dendrites over long distances are possible from much of this tissue, it is likely that shrinking due to inappropriate

osmotic balance and a variety of other issues causing tissue quality to suffer. Testing variations of this protocol that alter buffer concentrations and better maintain extracellular space (Cragg, 1980) will likely capture a state that is more physiologically accurate.

A nominal section thickness of ~60 nm made it possible to capture the complete larval zebrafish brain in ~18,000 sections. This nears the maximum number of sections compatible with the modified automated tape-collecting ultramicrotome presented here. Another sample was sectioned at ~50 nm, but less completely due to the increased number of sections required. Minimizing section thickness is an important factor in the success of axon and dendrite reconstructions (Briggman and Bock, 2012). A section thickness of 25–30 nm or less would increase confidence in the ability to capture near-complete neuronal circuit connectivity. This would permit Nyquist sampling of very small axons or dendrites, which become as small as 50–60 nm in diameter. Further modifications to automated tape-collecting microtomes will be necessary to test how thin complete larval zebrafish samples can be sectioned. Thicknesses of ≤30 nm are possible for mammalian brain tissues (Kasthuri *et al.*, under review), suggesting that the automated tape-collecting microtome itself will not be a limiting factor when tape-carrying capacity is increased.

All of the serial-section EM data presented here relied on back-scattered electron detection and was acquired at a rate at or under 1 megapixel per second ($Mpx \times s^{-1}$). This is far too slow for routine high-resolution imaging of even medium-sized portions of the larval zebrafish brain. However, back-scattered electron detection system upgrades with faster amplifiers are being introduced (Titze and Denk, 2013) and secondary electron detection methods are enabling parallel scanning of multiple beams (Eberle *et al.*, 2015). Whole-brain

serial-section EM in larval zebrafish will benefit substantially from the integration of these new imaging systems into the workflow.

One major limitation of the presented whole-brain serial-section EM dataset and section library is the inability to reliably discern gap junction-based electrical synapses. Furthermore, labeling specific neurons or populations of neurons would likely speed up reconstruction efforts. Future datasets can benefit from additional layers of information overlaid on top of the chemical synapses that can already be detected. Genetically encoded EM-compatible labels can be used to identify specific cells (Nagiel *et al.*, 2008), electrical synapses (Shu *et al.*, 2011), or specific synaptic proteins (Butko *et al.*, 2012; Paez-Segala *et al.*, 2015) using new techniques to knock-in label-tagged genes into the zebrafish genome (Zu *et al.*, 2013; Auer *et al.*, 2014).

Subsequent whole-brain serial-section EM datasets will be able to provide even more useful details about the structure of complete neuronal circuits with these changes.

4.2.4 Correspondence

Finding the same neurons from *in vivo* whole-brain fluorescence imaging in whole-brain serial-section EM datasets currently requires stack registration steps that rely on manual identification of cell nuclei. This is a difficult task in larval zebrafish with nearly pan-neuronal expression of only GCaMP indicators because nuclei appear dark as background signal rather than as a bright label. Using the *Tg(elavl3:H2B-mRFP)a9486* line to specifically label neuronal nuclei would help this process. However, manual stack alignment would benefit even more from the creation of a line with all nuclei labeled, as otherwise dim progenitor cells along the midline and cells surrounding the brain could be used to improve the alignment accuracy. This could be accomplished with the creation of a *Ubi*:H2B-mRFP transgenic line. Labelling nuclei with

fluorescent markers should accelerate and enhance correspondence between light- and EM-based datasets and may even enable an automated alignment in the future.

4.2.5 Analysis

Current tools for the analysis of most serial-section EM datasets rely on a large amount human interaction, making the process labor-intensive and expensive. Manual reconstruction alone can accomplish circuit reconstructions over long periods of time or with many annotators. However, efforts to automate image segmentation of serial-section EM datasets acquired at high resolution are improving considerably (Chklovskii *et al.*, 2010; Kaynig *et al.*, 2013; Krasowski *et al.*, 2015). Advances in this field and the development of new computational tools to integrate results across multiple resolutions will be very helpful for complete circuit reconstructions from whole-brain serial-section EM. Similarly, redesigning serial-section EM acquisition software for on-demand targeting of high-resolution imaging to areas based on manual and automated reconstruction progress has the potential to hasten the pace at which these endeavors can be conducted.

4.3 Conclusion

Producing datasets for combined whole-brain activity mapping and structural examination is now possible in larval zebrafish. These datasets have the potential to strengthen our understanding of neuronal function and its dependence on circuit architecture. Iterative improvements in the techniques used to acquire these datasets will facilitate faster production and higher quality results, eventually making it possible to routinely analyze the connectivity that links neurons identified in activity mapping experiments.

References

Ahrens MB, Engert F. 2015. Large-scale imaging in small brains. *Current Opinion in Neurobiology,* 32:78-86. doi:10.1016/j.conb.2015.01.007

Ahrens MB, Li JM, Orger MB, Robson DN, Schier AF, Engert F, Portugues R. 2012. Brain-wide neuronal dynamics during motor adaptation in zebrafish. *Nature,* 485:471-477. doi:10.1038/nature11057

Ahrens MB, Orger MB, Robson DN, Li JM, Keller PJ. 2013. Whole-brain functional imaging at cellular resolution using light-sheet microscopy. *Nature Methods,* 10:413-420. doi:10.1038/nmeth.2434

Akerboom J, Chen T-W, Wardill TJ, Tian L, Marvin JS, Mutlu S, Calderón NC, Esposti F, Borghuis BG, Sun XR, Gordus A, Orger MB, Portugues R, Engert F, Macklin JJ, Filosa A, Aggarwal A, Kerr RA, Takagi R, Kracun S, Shigetomi E, Khakh BS, Baier H, Lagnado L, Wang SSH, Bargmann CI, Kimmel BE, Jayaraman V, Svoboda K, Kim DS, Schreiter ER, Looger LL. 2012. Optimization of a GCaMP calcium indicator for neural activity imaging. *Journal of Neuroscience,* 32:13819-13840. doi:10.1523/JNEUROSCI.2601-12.2012

Anastassiou C, Perin R, Markram H, Koch C. 2011. Ephaptic coupling of cortical neurons. *Nature Neuroscience,* 14:217-223. doi:10.1038/nn.2727

Anderson JR, Jones BW, Watt CB, Shaw MV, Yang J-H, Demill D, Lauritzen JS, Lin Y, Rapp KD, Mastronarde D, Koshevoy P, Grimm B, Tasdizen T, Whitaker R, Marc RE. 2011. Exploring the retinal connectome. *Molecular Vision,* 17:355-379.

Auer TO, Duroure K, De Cian A, Concordet J-P, Del Bene F. 2014. Highly efficient CRISPR/Cas9-mediated knock-in in zebrafish by homology-independent DNA repair. *Genome Research,* 24:142-153. doi:10.1101/gr.161638.113

Bargmann CI, Marder E. 2013. From the connectome to brain function. *Nature Methods,* 10:483-490. doi:10.1038/nmeth.2451

Beier KT, Saunders A, Oldenburg IA, Miyamichi K, Akhtar N, Luo L, Whelan SPJ, Sabatini B, Cepko CL. 2011. Anterograde or retrograde transsynaptic labeling of CNS neurons with vesicular stomatitis virus vectors. *Proceedings of the National Academy of Sciences of the United States of America,* 108:15414-15419. doi:10.1073/pnas.1110854108

Bliss TVP, Lømo T. 1973. Long-lasting potentiation of synaptic transmission in the dentate area of the anaesthetized rabbit following stimulation of the perforant path. *Journal of Physiology,* 232:331-356. doi:10.1113/jphysiol.1973.sp010273

Bock DD, Lee W-CA, Kerlin AM, Andermann ML, Hood G, Wetzel AW, Yurgenson S, Soucy ER, Kim HS, Reid RC. 2011. Network anatomy and in vivo physiology of visual cortical neurons. *Nature,* 471:177-182. doi:10.1038/nature09802

Briggman KL, Bock DD. 2012. Volume electron microscopy for neuronal circuit reconstruction. *Current Opinion in Neurobiology,* 22:154-161. doi:10.1016/j.conb.2011.10.022

Briggman KL, Helmstaedter M, Denk W. 2011. Wiring specificity in the direction-selectivity circuit of the retina. *Nature,* 471:183-188. doi:10.1038/nature09818

Butko MT, Yang J, Geng Y, Kim HJ, Jeon NL, Shu X, Mackey MR, Ellisman MH, Tsien RY, Lin MZ. 2012. Fluorescent and photo-oxidizing TimeSTAMP tags track protein fates in light and electron microscopy. *Nature Neuroscience,* 15:1742-1751. doi:10.1038/nn.3246

Chapman S, Faulkner C, Kaiserli E, Garcia-Mata C, Savenkov EI, Roberts AG, Oparka KJ, Christie JM. 2008. The photoreversible fluorescent protein iLOV outperforms GFP as a reporter of plant virus infection. *Proceedings of the National Academy of Sciences of the United States of America,* 105:20038-20043. doi:10.1073/pnas.0807551105

Chen T-W, Wardill TJ, Sun Y, Pulver SR, Renninger SL, Baohan A, Schreiter ER, Kerr RA, Orger MB, Jayaraman V, Looger LL, Svoboda K, Kim DS. 2013. Ultrasensitive fluorescent proteins for imaging neuronal activity. *Nature,* 499:295-300. doi:10.1038/nature12354

Cheng A, Gonçalves JT, Golshani P, Arisaka K, Portera-Cailliau C. 2011. Simultaneous two-photon calcium imaging at different depths with spatiotemporal multiplexing. *Nature Methods,* 8:139-142. doi:10.1038/nmeth.1552

Cheng R-K, Lin Q, Krishnan S, Hildebrand DGC, Bianco IH, Kibat C, Engert F, Jesuthasan S. Neural circuitry mediating control of brain state by light. *(under review)*

Chklovskii DB, Vitaladevuni S, Scheffer LK. 2010. Semi-automated reconstruction of neural circuits using electron microscopy. *Current Opinion in Neurobiology,* 20:667-675. doi:10.1016/j.conb.2010.08.002

Cragg B. 1980. Preservation of extracellular space during fixation of the brain for electron microscopy. *Tissue and Cell,* 12:63-72. doi:10.1016/0040-8166(80)90052-X

Dacheux RF, Raviola E. 1986. The rod pathway in the rabbit retina: a depolarizing bipolar and amacrine cell. *Journal of Neuroscience,* 6:331-345.

Davidson BL, Breakefield XO. 2003. Viral vectors for gene delivery to the nervous system. *Nature Reviews Neuroscience,* 4:353-364. doi:10.1038/nrn1104

Davila HV, Salzberg BM, Cohen LB, Waggoner AS. 1973. A large change in axon fluorescence that provides a promising method for measuring membrane potential. *Nature New Biology,* 241:159-160. doi:10.1038/newbio241159a0

Deisseroth K, Schnitzer MJ. 2013. Engineering approaches to illuminating brain structure and dynamics. *Neuron,* 80:568-577. doi:10.1016/j.neuron.2013.10.032

Denk W, Horstmann H. 2004. Serial block-face scanning electron microscopy to reconstruct three-dimensional tissue nanostructure. *PLoS Biology,* 2:e329. doi:10.1371/journal.pbio.0020329

Detrich III HW, Westerfield M, Zon LI. 1998. Overview of the zebrafish system. *Methods in Cell Biology* (Vol. 59, pp. 3-10): Elsevier.

Douglas RJ, Martin KAC. 2004. Neuronal circuits of the neocortex. *Annual Review of Neuroscience,* 27:419-451. doi:10.1146/annurev.neuro.27.070203.144152

Eberle AL, Mikula S, Schalek R, Lichtman JW, Knothe Tate ML, Zeidler D. 2015. High-resolution, high-throughput imaging with a multibeam scanning electron microscope. *Journal of Microscopy* (in press). doi:10.1111/jmi.12224

Emran F, Rihel J, Adolph AR, Dowling JE. 2010. Zebrafish larvae lose vision at night. *Proceedings of the National Academy of Sciences of the United States of America,* 107:6034-6039. doi:10.1073/pnas.0914718107

Fan GY, Fujisaki H, Miyawaki A, Tsay RK, Tsien RY, Ellisman MH. 1999. Video-rate scanning two-photon excitation fluorescence microscopy and ratio imaging with Cameleons. *Biophysical Journal,* 76:2412-2420. doi:10.1016/S0006-3495(99)77396-0

Feierstein CE, Portugues R, Orger MB. 2014. Seeing the whole picture: A comprehensive imaging approach to functional mapping of circuits in behaving zebrafish. *Neuroscience* (in press). doi:10.1016/j.neuroscience.2014.11.046

Fetcho JR, O'Malley DM. 1995. Visualization of active neural circuitry in the spinal cord of intact zebrafish. *Journal of Neurophysiology,* 73:399-406.

Fetcho JR, O'Malley DM. 1997. Imaging neuronal networks in behaving animals. *Current Opinion in Neurobiology,* 7:832-838. doi:10.1016/S0959-4388(97)80143-2

Finck H. 1960. Epoxy resins in electron microscopy. *Journal of Biophysical and Biochemical Cytology,* 7:27-30.

Friedlander MJ, Lin CS, Stanford LR, Sherman SM. 1981. Morphology of functionally identified neurons in lateral geniculate nucleus of the cat. *Journal of Neurophysiology,* 46:80-129.

Friedrich RW, Genoud C, Wanner AA. 2013. Analyzing the structure and function of neuronal circuits in zebrafish. *Frontiers in Neural Circuits,* 7:71. doi:10.3389/fncir.2013.00071

Friedrich RW, Jacobson GA, Zhu P. 2010. Circuit neuroscience in zebrafish. *Current Biology,* 20:R371-R381. doi:10.1016/j.cub.2010.02.039

Golgi C. 1873. Sulla struttura della sostanza grigia del cervello. *Gazzetta Medica Italiana. Lombardia,* 33:244-246.

Grant PK, Moens CB. 2010. The neuroepithelial basement membrane serves as a boundary and a substrate for neuron migration in the zebrafish hindbrain. *Neural Development,* 5:9. doi:10.1186/1749-8104-5-9

Grewe BF, Helmchen F. 2009. Optical probing of neuronal ensemble activity. *Current Opinion in Neurobiology,* 19:520-529. doi:10.1016/j.conb.2009.09.003

Grewe BF, Langer D, Kasper H, Kampa BM, Helmchen F. 2010. High-speed in vivo calcium imaging reveals neuronal network activity with near-millisecond precision. *Nature Methods,* 7:399-405. doi:10.1038/nmeth.1453

Grewe BF, Voigt FF, van 't Hoff M, Helmchen F. 2011. Fast two-layer two-photon imaging of neuronal cell populations using an electrically tunable lens. *Biomedical Optics Express,* 2:2035-2046. doi:10.1364/BOE.2.002035

Grienberger C, Konnerth A. 2012. Imaging calcium in neurons. *Neuron,* 73:862-885. doi:10.1016/j.neuron.2012.02.011

Gutzman JH, Graeden EG, Lowery LA, Holley HS, Sive H. 2008. Formation of the zebrafish midbrain-hindbrain boundary constriction requires laminin-dependent basal constriction. *Mechanisms of Development,* 125:974-983. doi:10.1016/j.mod.2008.07.004

Hamos JE, Van Horn SC, Raczkowski D, Sherman SM. 1987. Synaptic circuits involving an individual retinogeniculate axon in the cat. *Journal of Comparative Neurology,* 259:165-192. doi:10.1002/cne.902590202

Hayat MA. 1981. *Fixation for Electron Microscopy*. Academic Press.

Hayworth KJ, Kasthuri N, Schalek R, Lichtman JW. 2006. Automating the collection of ultrathin serial sections for large volume TEM reconstructions. *Microscopy and Microanalysis,* 12:86-87. doi:10.1017/S1431927606066268

Hayworth KJ, Morgan JL, Schalek R, Berger DR, Hildebrand DGC, Lichtman JW. 2014. Imaging ATUM ultrathin section libraries with WaferMapper: a multi-scale approach to EM reconstruction of neural circuits. *Frontiers in Neural Circuits,* 8:68. doi:10.3389/fncir.2014.00068

Helmstaedter M, Briggman KL, Denk W. 2008. 3D structural imaging of the brain with photons and electrons. *Current Opinion in Neurobiology,* 18:633-641. doi:10.1016/j.conb.2009.03.005

Helmstaedter M, Briggman KL, Turaga SC, Jain V, Seung HS, Denk W. 2013. Connectomic reconstruction of the inner plexiform layer in the mouse retina. *Nature,* 500:168-174. doi:10.1038/nature12346

Higashijima S-i, Masino MA, Mandel G, Fetcho JR. 2003. Imaging neuronal activity during zebrafish behavior with a genetically encoded calcium indicator. *Journal of Neurophysiology,* 90:3986-3997. doi:10.1152/jn.00576.2003

Higashijima S-i, Okamoto H, Ueno N, Hotta Y, Eguchi G. 1997. High-frequency generation of transgenic zebrafish which reliably express GFP in whole muscles or the whole body by using promoters of zebrafish origin. *Developmental Biology,* 192:289-299. doi:10.1006/dbio.1997.8779

Hinz FI, Aizenberg M, Tushev G, Schuman EM. 2013. Protein synthesis-dependent associative long-term memory in larval zebrafish. *Journal of Neuroscience,* 33:15382-15387. doi:10.1523/JNEUROSCI.0560-13.2013

Hubel DH. 1957. Tungsten microelectrode for recording from single units. *Science,* 125:549-550.

Hubel DH, Wiesel TN. 1959. Receptive fields of single neurones in the cat's striate cortex. *Journal of Physiology,* 148:574-591. doi:10.1113/jphysiol.1959.sp006308

Huisken J, Swoger J, Del Bene F, Wittbrodt J, Stelzer EHK. 2004. Optical sectioning deep inside live embryos by selective plane illumination microscopy. *Science,* 305:1007-1009. doi:10.1126/science.1100035

Jaffe DB, Johnston D, Lasser-Ross N, Lisman JE, Miyakawa H, Ross WN. 1992. The spread of Na+ spikes determines the pattern of dendritic Ca2+ entry into hippocampal neurons. *Nature,* 357:244-246. doi:10.1038/357244a0

Kandel ER, Schwartz JH, Jessell TM. 2000. *Principles of Neural Science*. 3rd ed. McGraw-Hill.

Karlsson J, von Hofsten J, Olsson P-E. 2001. Generating transparent zebrafish: a refined method to improve detection of gene expression during embryonic development. *Marine Biotechnology,* 3:522-527. doi:10.1007/s1012601-0053-4

Kasthuri N, Hayworth KJ, Berger DR, Schalek RL, Conchello JA, Knowles-Barley S, Lee D, Vázquez-Reina A, Kaynig V, Jones TR, Roberts M, Morgan JL, Tapia JC, Seung HS, Roncal WG, Vogelstein JT, Burns R, Sussman DL, Priebe CE, Pfister H, Lichtman JW. 2015. Saturated reconstruction of a small volume of neocortex. *under review*

Katona G, Szalay G, Maák P, Kaszás A, Veress M, Hillier D, Chiovini B, Vizi E, Roska B, Rózsa B. 2012. Fast two-photon in vivo imaging with three-dimensional random-access scanning in large tissue volumes. *Nature Methods,* 9:201-208. doi:10.1038/nmeth.1851

Kawakami K. 2007. Tol2: a versatile gene transfer vector in vertebrates. *Genome Biology,* 8:S7. doi:10.1186/gb-2007-8-s1-s7

Kaynig V, Vazquez-Reina A, Knowles-Barley S, Roberts M, Jones TR, Kasthuri N, Miller E, Lichtman J, Pfister H. 2013. Large-scale automatic reconstruction of neuronal processes from electron microscopy images. *arXiv*1303.7186.

Keller PJ, Ahrens MB. 2015. Visualizing whole-brain activity and development at the single-cell level using light-sheet microscopy. *Neuron,* 85:462-483. doi:10.1016/j.neuron.2014.12.039

Keller PJ, Schmidt AD, Wittbrodt J, Stelzer EHK. 2008. Reconstruction of zebrafish early embryonic development by scanned light sheet microscopy. *Science,* 322:1065-1069. doi:10.1126/science.1162493

Kerlin AM, Andermann ML, Berezovskii VK, Reid RC. 2010. Broadly tuned response properties of diverse inhibitory neuron subtypes in mouse visual cortex. *Neuron,* 67:858-871. doi:10.1016/j.neuron.2010.08.002

Kerr JND, Denk W. 2008. Imaging in vivo: watching the brain in action. *Nature Reviews Neuroscience,* 9:195-205. doi:10.1038/nrn2338

Kim C-H, Ueshima E, Muraoka O, Tanaka H, Yeo S-Y, Huh T-L, Miki N. 1996. Zebrafish elav/HuC homologue as a very early neuronal marker. *Neuroscience Letters,* 216:109-112. doi:10.1016/0304-3940(96)13021-4

Kim CK, Miri A, Leung LC, Berndt A, Mourrain P, Tank DW, Burdine RD. 2014. Prolonged, brain-wide expression of nuclear-localized GCaMP3 for functional circuit mapping. *Frontiers in Neural Circuits,* 8:138. doi:10.3389/fncir.2014.00138

Kimmel CB, Sessions SK, Kimmel RJ. 1981. Morphogenesis and synaptogenesis of the zebrafish mauthner neuron. *Journal of Comparative Neurology,* 198:101-120. doi:10.1002/cne.901980110

Knöpfel T. 2012. Genetically encoded optical indicators for the analysis of neuronal circuits. *Nature Reviews Neuroscience,* 13:687-700. doi:10.1038/nrn3293

Knöpfel T, Díez-García J, Akemann W. 2006. Optical probing of neuronal circuit dynamics: genetically encoded versus classical fluorescent sensors. *Trends in Neurosciences,* 29:160-166. doi:10.1016/j.tins.2006.01.004

Knott G, Marchman H, Wall D, Lich B. 2008. Serial section scanning electron microscopy of adult brain tissue using focused ion beam milling. *Journal of Neuroscience,* 28:2959-2964. doi:10.1523/JNEUROSCI.3189-07.2008

Knott GW, Holtmaat A, Trachtenberg JT, Svoboda K, Welker E. 2009. A protocol for preparing GFP-labeled neurons previously imaged in vivo and in slice preparations for light and electron microscopic analysis. *Nature Protocols,* 4:1145-1156. doi:10.1038/nprot.2009.114

Ko H, Cossell L, Baragli C, Antolik J, Clopath C, Hofer SB, Mrsic-Flogel TD. 2013. The emergence of functional microcircuits in visual cortex. *Nature,* 496:96-100. doi:10.1038/nature12015

Ko H, Hofer SB, Pichler B, Buchanan KA, Sjöström PJ, Mrsic-Flogel TD. 2011. Functional specificity of local synaptic connections in neocortical networks. *Nature,* 473:87-91. doi:10.1038/nature09880

Krasowski N, Beier T, Knott G, Koethe U, Hamprecht F, Kreshuk A. 2015. Improving 3D EM data segmentation by joint optimization over boundary evidence and biological priors. *IEEE ISBIin press*.

Laale HW. 1977. The biology and use of zebrafish, Brachydanio rerio in fisheries research: a literature review. *Journal of Fish Biology,* 10:121-173. doi:10.1111/j.1095-8649.1977.tb04049.x

Lee A, Mathuru AS, Teh C, Kibat C, Korzh V, Penney TB, Jesuthasan S. 2010. The habenula prevents helpless behavior in larval zebrafish. *Current Biology,* 20:2211–2216. doi:10.1016/j.cub.2010.11.025

Levoy M, Ng R, Adams A, Footer M, Horowitz M. 2006. Light field microscopy. *ACM Transactions on Graphics,* 25:924-934. doi:10.1145/1141911.1141976

Lichtman JW, Denk W. 2011. The big and the small: challenges of imaging the brain's circuits. *Science,* 334:618-623. doi:10.1126/science.1209168

Llinás RR. 2014. Intrinsic electrical properties of mammalian neurons and CNS function: a historical perspective. *Frontiers in Cellular Neuroscience,* 8:320. doi:10.3389/fncel.2014.00320

Looger LL, Griesbeck O. 2012. Genetically encoded neural activity indicators. *Current Opinion in Neurobiology,* 22:18-23. doi:10.1016/j.conb.2011.10.024

Luft JH. 1973. Embedding media—old and new. In J. K. Koehler (Ed.), *Advanced Techniques in Biological Electron Microscopy* (pp. 1-34): Springer-Verlag.

Ma L-H, Punnamoottil B, Rinkwitz S, Baker R. 2009. Mosaic hoxb4a neuronal pleiotropism in zebrafish caudal hindbrain. *PLoS ONE,* 4:e5944. doi:10.1371/journal.pone.0005944

Marblestone AH, Zamft BM, Maguire YG, Shapiro MG, Cybulski TR, Glaser JI, Amodei D, Stranges PB, Kalhor R, Dalrymple DA, Seo D, Alon E, Maharbiz MM, Carmena JM, Rabaey JM, Boyden ES, Church GM, Kording KP. 2013. Physical principles for scalable neural recording. *Frontiers in Computational Neuroscience,* 7:137. doi:10.3389/fncom.2013.00137

Marder E, O'Leary T, Shruti S. 2014. Neuromodulation of circuits with variable parameters: single neurons and small circuits reveal principles of state-dependent and robust neuromodulation. *Annual Review of Neuroscience,* 37:329-346. doi:10.1146/annurev-neuro-071013-013958

Masino MA, Fetcho JR. 2005. Fictive swimming motor patterns in wild type and mutant larval zebrafish. *Journal of Neurophysiology,* 93:3177-3188. doi:10.1152/jn.01248.2004

Metcalfe WK, Kimmel CB, Schabtach E. 1985. Anatomy of the posterior lateral line system in young larvae of the zebrafish. *Journal of Comparative Neurology,* 233:377-389. doi:10.1002/cne.902330307

Mikula S, Binding J, Denk W. 2012. Staining and embedding the whole mouse brain for electron microscopy. *Nature Methods,* 9:1198-1201. doi:10.1038/nmeth.2213

Miner JH, Yurchenco PD. 2004. Laminin functions in tissue morphogenesis. *Annual Review of Cell and Developmental Biology,* 20:255-284. doi:10.1146/annurev.cellbio.20.010403.094555

Monk KR, Naylor SG, Glenn TD, Mercurio S, Perlin JR, Dominguez C, Moens CB, Talbot WS. 2009. A G Protein-coupled receptor is essential for Schwann cells to initiate myelination. *Science,* 325:1402-1405. doi:10.1126/science.1173474

Muto A, Ohkura M, Kotani T, Higashijima S-i, Nakai J, Kawakami K. 2011. Genetic visualization with an improved GCaMP calcium indicator reveals spatiotemporal activation of the spinal motor neurons in zebrafish. *Proceedings of the National Academy of Sciences of the United States of America,* 108:5425-5430. doi:10.1073/pnas.1000887108

Nagiel A, Andor-Ardo D, Hudspeth AJ. 2008. Specificity of Afferent Synapses onto Plane-Polarized Hair Cells in the Posterior Lateral Line of the Zebrafish. *Journal of Neuroscience,* 28:8442-8453. doi:10.1523/JNEUROSCI.2425-08.2008

Nakai J, Ohkura M, Imoto K. 2001. A high signal-to-noise Ca2+ probe composed of a single green fluorescent protein. *Nature Biotechnology,* 19:137-141. doi:10.1038/84397

Nakamura C, Burgess JG, Sode K, Matsunaga T. 1995. An iron-regulated gene, magA, encoding an iron transport protein of Magnetospirillum sp. strain AMB-1. *Journal of Biological Chemistry,* 270:28392-28396.

Nikolenko V, Watson BO, Araya R, Woodruff A, Peterka DS, Yuste R. 2008. SLM microscopy: scanless two-photon imaging and photostimulation using spatial light modulators. *Frontiers in Neural Circuits,* 2:5. doi:10.3389/neuro.04.005.2008

Nusslein-Volhard C, Dahm R. 2002. *Zebrafish: A Practical Approach*. Oxford.

O'Malley DM, Kao Y-H, Fetcho JR. 1996. Imaging the functional organization of zebrafish hindbrain segments during escape behaviors. *Neuron,* 17:1145-1155. doi:10.1016/S0896-6273(00)80246-9

Ohki K, Chung S, Ch'ng YH, Kara P, Reid RC. 2005. Functional imaging with cellular resolution reveals precise micro-architecture in visual cortex. *Nature,* 433:597-603. doi:10.1038/nature03274

Ohki K, Chung S, Kara P, Hübener M, Bonhoeffer T, Reid RC. 2006. Highly ordered arrangement of single neurons in orientation pinwheels. *Nature,* 442:925-928. doi:10.1038/nature05019

Orger MB, Kampff AR, Severi KE, Bollmann JH, Engert F. 2008. Control of visually guided behavior by distinct populations of spinal projection neurons. *Nature Neuroscience,* 11:327-333. doi:10.1038/nn2048

Packer AM, Roska B, Häusser M. 2013. Targeting neurons and photons for optogenetics. *Nature Neuroscience,* 16:805-815. doi:10.1038/nn.3427

Packer AM, Russell LE, Dalgleish HWP, Häusser M. 2015. Simultaneous all-optical manipulation and recording of neural circuit activity with cellular resolution in vivo. *Nature Methods,* 12:140-146. doi:10.1038/nmeth.3217

Paez-Segala MG, Sun MG, Shtengel G, Viswanathan S, Baird MA, Macklin JJ, Patel R, Allen JR, Howe ES, Piszczek G, Hess HF, Davidson MW, Wang Y, Looger LL. 2015. Fixation-resistant photoactivatable fluorescent proteins for CLEM. *Nature Methods,* 12:215-218. doi:10.1038/nmeth.3225

Panier T, Romano SA, Olive R, Pietri T, Sumbre G, Candelier R, Debrégeas G. 2013. Fast functional imaging of multiple brain regions in intact zebrafish larvae using selective plane illumination microscopy. *Frontiers in Neural Circuits,* 7:65. doi:10.3389/fncir.2013.00065

Perea G, Sur M, Araque A. 2014. Neuron-glia networks: integral gear of brain function. *Frontiers in Cellular Neuroscience,* 8:378. doi:10.3389/fncel.2014.00378

Peters A, Palay SL, Webster Hd. 1991. *The Fine Structure of the Nervous System: Neurons and Their Supporting Cells*. 3 ed. Oxford.

Petreanu L, Huber D, Sobczyk A, Svoboda K. 2007. Channelrhodopsin-2–assisted circuit mapping of long-range callosal projections. *Nature Neuroscience,* 10:663-668. doi:10.1038/nn1891

Pogoda H-M, Sternheim N, Lyons DA, Diamond B, Hawkins TA, Woods IG, Bhatt DH, Franzini-Armstrong C, Dominguez C, Arana N, Jacobs J, Nix R, Fetcho JR, Talbot WS. 2006. A genetic screen identifies genes essential for development of myelinated axons in zebrafish. *Developmental Biology,* 298:118-131. doi:10.1016/j.ydbio.2006.06.021

Portugues R, Engert F. 2009. The neural basis of visual behaviors in the larval zebrafish. *Current Opinion in Neurobiology,* 19:644-647. doi:10.1016/j.conb.2009.10.007

Portugues R, Feierstein CE, Engert F, Orger MB. 2014. Whole-brain activity maps reveal stereotyped, distributed networks for visuomotor behavior. *Neuron,* 81:1328-1343. doi:10.1016/j.neuron.2014.01.019

Portugues R, Severi KE, Wyart C, Ahrens MB. 2013. Optogenetics in a transparent animal: circuit function in the larval zebrafish. *Current Opinion in Neurobiology,* 23:119-126. doi:10.1016/j.conb.2012.11.001

Pozo K, Goda Y. 2010. Unraveling mechanisms of homeostatic synaptic plasticity. *Neuron,* 66:337-351. doi:10.1016/j.neuron.2010.04.028

Prevedel R, Yoon Y-G, Hoffmann M, Pak N, Wetzstein G, Kato S, Schrödel T, Raskar R, Zimmer M, Boyden ES, Vaziri A. 2014. Simultaneous whole-animal 3D imaging of neuronal activity using light-field microscopy. *Nature Methods,* 11:727-730. doi:10.1038/nmeth.2964

Prober DA, Rihel J, Onah AA, Sung R-J, Schier AF. 2006. Hypocretin/orexin overexpression induces an insomnia-like phenotype in zebrafish. *Journal of Neuroscience,* 26:13400-13410. doi:10.1523/JNEUROSCI.4332-06.2006

Ramón y Cajal S. 1904. *Textura del Sistema Nervioso del Hombre y de los Vertebrados*. Moya.

Randlett O, Naumann EA, Portugues R, Wee C, Schoppik D, Lacoste A, Riegler C, Engert F, F. SA. Whole-brain activity mapping of freely swimming zebrafish in an open source brain atlas. *submitted*

Rickgauer JP, Deisseroth K, Tank DW. 2014. Simultaneous cellular-resolution optical perturbation and imaging of place cell firing fields. *Nature Neuroscience,* 17:1816-1824. doi:10.1038/nn.3866

Roberts JA, Miguel-Escalada I, Slovik KJ, Walsh KT, Hadzhiev Y, Sanges R, Stupka E, Marsh EK, Balciuniene J, Balciunas D, Müller F. 2014. Targeted transgene integration overcomes variability of position effects in zebrafish. *Development,* 141:715-724. doi:10.1242/dev.100347

Saalfeld S, Cardona A, Hartenstein V, Tomančák P. 2009. CATMAID: collaborative annotation toolkit for massive amounts of image data. *Bioinformatics,* 25:1984-1986. doi:10.1093/bioinformatics/btp266

Saalfeld S, Cardona A, Hartenstein V, Tomančák P. 2010. As-rigid-as-possible mosaicking and serial section registration of large ssTEM datasets. *Bioinformatics,* 26:i57-i63. doi:10.1093/bioinformatics/btq219

Sabatini BL, Maravall M, Svoboda K. 2001. Ca2+ signaling in dendritic spines. *Current Opinion in Neurobiology,* 11:349-356. doi:10.1016/S0959-4388(00)00218-X

Schalek R, Kasthuri N, Hayworth K, Berger D, Tapia J, Morgan J, Turaga S, Fagerholm E, Seung H, Lichtman J. 2011. Development of high-throughput, high-resolution 3D reconstruction of large-volume biological tissue using automated tape collection ultramicrotomy and scanning electron microscopy. *Microscopy and Microanalysis,* 17:966-967. doi:10.1017/S1431927611005708

Schindelin J, Arganda-Carreras I, Frise E, Kaynig V, Longair M, Pietzsch T, Preibisch S, Rueden C, Saalfeld S, Schmid B, Tinevez J-Y, White DJ, Hartenstein V, Eliceiri K, Tomancak P, Cardona A. 2012. Fiji: an open-source platform for biological-image analysis. *Nature Methods,* 9:676-682. doi:10.1038/nmeth.2019

Schmidt R, Strähle U, Scholpp S. 2013. Neurogenesis in zebrafish from embryo to adult. *Neural Development,* 8:3. doi:10.1186/1749-8104-8-3

Schmitt EA, Dowling JE. 1994. Early-eye morphogenesis in the zebrafish, Brachydanio rerio. *Journal of Comparative Neurology,* 344:532-542. doi:10.1002/cne.903440404

Schmitt EA, Dowling JE. 1999. Early retinal development in the zebrafish, Danio rerio: light and electron microscopic analyses. *Journal of Comparative Neurology,* 404:515-536. doi:10.1002/(SICI)1096-9861(19990222)404:4<515::AID-CNE8>3.0.CO;2-A

Shenoy KV, Sahani M, Churchland MM. 2013. Cortical control of arm movements: a dynamical systems perspective. *Annual Review of Neuroscience,* 36:337-359. doi:10.1146/annurev-neuro-062111-150509

Shepherd GMG, Stepanyants A, Bureau I, Chklovskii DB, Svoboda K. 2005. Geometric and functional organization of cortical circuits. *Nature Neuroscience,* 8:782-790. doi:10.1038/nn1447

Shu X, Lev-Ram V, Deerinck TJ, Qi Y, Ramko EB, Davidson MW, Jin Y, Ellisman MH, Tsien RY. 2011. A genetically encoded tag for correlated light and electron microscopy of intact cells, tissues, and organisms. *PLoS Biology,* 9:e1001041. doi:10.1371/journal.pbio.1001041

Song S, Sjöström PJ, Reigl M, Nelson S, Chklovskii DB. 2005. Highly nonrandom features of synaptic connectivity in local cortical circuits. *PLoS Biology,* 3:e68. doi:10.1371/journal.pbio.0030068

Sorra KE, Harris KM. 1998. Stability in synapse number and size at 2 hr after long-term potentiation in hippocampal area CA1. *Journal of Neuroscience,* 18:658-671.

Spira ME, Hai A. 2013. Multi-electrode array technologies for neuroscience and cardiology. *Nature Nanotechnology,* 8:83-94. doi:10.1038/nnano.2012.265

Sterling P. 1983. Microcircuitry of the cat retina. *Annual Review of Neuroscience,* 6:149-185. doi:10.1146/annurev.ne.06.030183.001053

Streisinger G, Walker C, Dower N, Knauber D, Singer F. 1981. Production of clones of homozygous diploid zebra fish (Brachydanio rerio). *Nature,* 291:293-296. doi:10.1038/291293a0

Subach FV, Patterson GH, Renz M, Lippincott-Schwartz J, Verkhusha VV. 2010. Bright monomeric photoactivatable red fluorescent protein for two-color super-resolution sptPALM of live cells. *Journal of the American Chemical Society,* 132:6481-6491. doi:10.1021/ja100906g

Swinburne IA, Mosaliganti KR, Hildebrand DGC, Al-Obeidi E, Engert F, Lichtman JW, Megason SG. Lamellar junctions in the endolymphatic sac act as a relief valve to regulate inner ear pressure. *(submitted)*

Tapia JC, Kasthuri N, Hayworth KJ, Schalek R, Lichtman JW, Smith SJ, Buchanan J. 2012. High-contrast en bloc staining of neuronal tissue for field emission scanning electron microscopy. *Nature Protocols,* 7:193-206. doi:10.1038/nprot.2011.439

Tian L, Hires SA, Looger LL. 2012. Imaging neuronal activity with genetically encoded calcium indicators. *Cold Spring Harbor Protocols,* 2012:647-656. doi:10.1101/pdb.top069609

Tian L, Hires SA, Mao T, Huber D, Chiappe ME, Chalasani SH, Petreanu L, Akerboom J, McKinney SA, Schreiter ER, Bargmann CI, Jayaraman V, Svoboda K, Looger LL. 2009. Imaging neural activity in worms, flies and mice with improved GCaMP calcium indicators. *Nature Methods,* 6:875-881. doi:10.1038/nmeth.1398

Titze B, Denk W. 2013. Automated in-chamber specimen coating for serial block-face electron microscopy. *Journal of Microscopy,* 250:101-110. doi:10.1111/jmi.12023

Turner MH, Ullmann JFP, Kay AR. 2012. A method for detecting molecular transport within the cerebral ventricles of live zebrafish (Danio rerio) larvae. *Journal of Physiology,* 590:2233-2240. doi:10.1113/jphysiol.2011.225896

Vladimirov N, Mu Y, Kawashima T, Bennett DV, Yang C-T, Looger LL, Keller PJ, Freeman J, Ahrens MB. 2014. Light-sheet functional imaging in fictively behaving zebrafish. *Nature Methods,* 11:883-884. doi:10.1038/nmeth.3040

White JG, Southgate E, Thomson JN, Brenner S. 1986. The structure of the nervous system of the nematode Caenorhabditis elegans. *Philosophical Transactions of the Royal Society B: Biological Sciences,* 314:1-340. doi:10.1098/rstb.1986.0056

White RM, Sessa A, Burke C, Bowman T, LeBlanc J, Ceol C, Bourque C, Dovey M, Goessling W, Burns CE, Zon LI. 2008. Transparent adult zebrafish as a tool for in vivo transplantation analysis. *Cell Stem Cell,* 2:183-189. doi:10.1016/j.stem.2007.11.002

Wickersham IR, Finke S, Conzelmann K-K, Callaway EM. 2007a. Retrograde neuronal tracing with a deletion-mutant rabies virus. *Nature Methods,* 4:47-49. doi:10.1038/nmeth999

Wickersham IR, Lyon DC, Barnard RJO, Mori T, Finke S, Conzelmann K-K, Young JAT, Callaway EM. 2007b. Monosynaptic restriction of transsynaptic tracing from single, genetically targeted neurons. *Neuron,* 53:639-647. doi:10.1016/j.neuron.2007.01.033

Xiao T, Baier H. 2007. Lamina-specific axonal projections in the zebrafish tectum require the type IV collagen Dragnet. *Nature Neuroscience,* 10:1529-1537. doi:10.1038/nn2002

Yuste R, Majewska A, Holthoff K. 2000. From form to function: calcium compartmentalization in dendritic spines. *Nature Neuroscience,* 3:653-659. doi:10.1038/76609

Zhu P, Narita Y, Bundschuh ST, Fajardo O, Schärer Y-P, Chattopadhyaya B, Bouldoires EA, Stepien AE, Deisseroth K, Arber S, Sprengel R, Rijli FM, Friedrich RW. 2009. Optogenetic dissection of neuronal circuits in zebrafish using viral gene transfer and the Tet system. *Frontiers in Neural Circuits,* 3:21. doi:10.3389/neuro.04.021.2009

Zipfel WR, Williams RM, Webb WW. 2003. Nonlinear magic: multiphoton microscopy in the biosciences. *Nature Biotechnology,* 21:1369-1377. doi:10.1038/nbt899

Zu Y, Tong X, Wang Z, Liu D, Pan R, Li Z, Hu Y, Luo Z, Huang P, Wu Q, Zhu Z, Zhang B, Lin S. 2013. TALEN-mediated precise genome modification by homologous recombination in zebrafish. *Nature Methods,* 10:329-331. doi:10.1038/nmeth.2374